

Faculty of Science and Technology

Department of Chemistry

# Solvent effects with Multiwavelets

*kje-3900*

—

**Rune Sørland Monstad**

*Master thesis in Chemistry – November 2017*





# Contents

<b>1</b>	<b>Introduction</b>	<b>7</b>
1.1	The Schrödinger equation . . . . .	7
1.2	Quantum Chemistry . . . . .	8
1.3	Structure . . . . .	9
<b>2</b>	<b>Basis sets</b>	<b>11</b>
2.1	Introduction to function basis . . . . .	12
2.2	Atom-centered basis functions . . . . .	12
2.2.1	Gaussian Type Orbitals (GTOs) . . . . .	14
2.2.2	Gaussian contractions . . . . .	15
2.3	MultiResolution Analysis (MRA) . . . . .	16
2.3.1	The Haar basis . . . . .	16
2.3.2	The multiwavelet basis . . . . .	22
2.4	Multiwavelet vs. Gaussian Type Orbitals . . . . .	24
<b>3</b>	<b>QM-methods</b>	<b>25</b>
3.1	The electronic Schrödinger equation . . . . .	26
3.2	The Hartree-Fock method . . . . .	27
3.2.1	General considerations . . . . .	27
3.2.2	Hartree-Fock method with Gaussian Type Orbitals . . . . .	30
3.2.3	Hartree-Fock method with multi-wavelets . . . . .	31
3.3	Density Functional Theory . . . . .	32
3.4	Energy calculation with multi-wavelets . . . . .	34
3.4.1	Energy calculations for Hartree-Fock . . . . .	34
3.4.2	Energy calculations for Density Functional Theory . . . . .	35
<b>4</b>	<b>Solvation Models</b>	<b>37</b>
4.1	Solvation Models . . . . .	37
4.1.1	The all inclusive discrete method . . . . .	38
4.1.2	Continuum models . . . . .	39
4.2	PCM for GTO . . . . .	40

---

4.2.1	Cavity formulation using Tesserars . . . . .	41
4.3	PCM for MW . . . . .	43
4.3.1	Solvent effect potential inclusion in HF . . . . .	44
4.3.2	Solvent effect potential inclusion in DFT . . . . .	44
4.4	Solvent energy with MW . . . . .	44
4.4.1	Solvent energy calculations for wavelet Hartree-Fock . . . . .	45
4.4.2	Solvent energy calculations for wavelet Density Functional Theory . . . . .	45
<b>5</b>	<b>Implementation</b> . . . . .	<b>47</b>
5.1	Cavity implementation . . . . .	47
5.1.1	The interlocking sphere approach and representation of $\varepsilon(r)$ . . . . .	48
5.2	SCF implementation . . . . .	49
5.2.1	Pilot code . . . . .	50
5.2.2	Full implementation . . . . .	53
<b>6</b>	<b>Results</b> . . . . .	<b>55</b>
6.1	Pilot code . . . . .	55
6.2	Full implementation . . . . .	56
6.2.1	Solvent energy . . . . .	57
6.2.2	Solvent dipole Moment . . . . .	59
6.3	Concluding remarks and ideas for improvement . . . . .	60

## Abbreviations

The following abbreviations are all defined in the text. This list is made to allow for easy reference (alphabetical).

<b>ASC</b> Apparent Surface Charge .....	56
<b>AO</b> Atomic Orbital.....	30
<b>BO</b> Born-Oppenheimer approximation.....	26
<b>CC</b> Couple-Cluster.....	25
<b>DFT</b> Density Functional Theory .....	50
<b>GIAO</b> Gauge Including Atomic Orbitals .....	24
<b>GTF</b> Gaussian-Type Function.....	12
<b>GTO</b> Gaussian-Type Orbital.....	47
<b>HF</b> Hartree-Fock.....	57
<b>HTM</b> Hierarchical Triangular Mesh .....	42
<b>KAIN</b> Krylov subspace Accelerated Inexact Newton Method.....	53
<b>LCAO</b> Linear Combination of Atomic Orbitals.....	30
<b>MM</b> Molecular Mechanic.....	38
<b>MO</b> Molecular Orbital .....	30

---

<b>MPn</b> Møller-Plesset perturbation .....	25
<b>MRA</b> Multiresolution Analysis .....	16
<b>MW</b> MultiWavelet .....	55
<b>PCM</b> Polarizable Continuum model .....	57
<b>PDE</b> Partial Differential Equation .....	11
<b>QM</b> Quantum Mechanic .....	38
<b>SCF</b> Self-Consistent Field .....	55
<b>SE</b> Schrödinger Equation .....	41
<b>STF</b> Slater-Type Function .....	12
<b>SVPE</b> Surface and Volume Polarization of Electrostatics .....	55
<b>vdW</b> van der Waals .....	60

# Chapter 1

## Introduction

### Contents

---

1.1	The Schrödinger equation . . . . .	7
1.2	Quantum Chemistry . . . . .	8
1.3	Structure . . . . .	9

---

### 1.1 The Schrödinger equation

Modern computational chemistry is, usually, based on the Schrödinger Equation (SE) postulated by Erwin Schrödinger in 1926. The equation was made to model the spectrum of the Hydrogen atom. Although the SE is only analytically solvable for one electron systems ( $H$ ,  $He^+$ ,  $H_2^+$  etc.), it soon became apparent that the equation also could be used for larger systems. The solutions  $\Psi$  of the time independent SE

$$\hat{H}\Psi(\vec{x}) = E\Psi(\vec{x}) \tag{1.1}$$

are called wave functions; they contain all the information about a system. The Hamiltonian  $\hat{H}$  is the total energy operator, and the eigenvalue  $E$  the total energy.  $\Psi$  is an eigenfunction of the Hamiltonian, and is generally a complex-valued multi-dimensional function.  $\Psi = \Psi(\vec{x}_1, \vec{x}_2, \dots, \vec{x}_n)$  where  $\vec{x}_i = (\vec{r}_i, s_i)$  denotes, respectively, the position and spin of the particle,  $n$  is the number for particles. This means that the dimensionality of the wavefunction increases with a factor of 4 (if spin is regarded as a dimension in its own right) with respect to the number of particles.

The specific information of interest can be determined by operators and

their respective expectation value.

$$\langle \hat{\omega} \rangle = \frac{\langle \Psi | \hat{\omega} | \Psi \rangle}{\langle \Psi | \Psi \rangle} \quad (1.2)$$

Throughout the rest of this thesis, unless otherwise stated, atomic units have been used. This means that  $j_0 = \hbar = m_e = 1$ , distances are expressed in terms of the Bohr radius ( $a_0$ ) and energies are expressed in Hartree ( $E_h$ ).

## 1.2 Quantum Chemistry

The main focus of this thesis is how a solvent effect the total energy of a system. For experimental chemists, it is important to have precise calculations on molecules in an environment that is as realistic as possible. This is why many computational chemists work to improve their codes to include solvent effect, and it is the reason why it is implemented in MRCHEM [1].

A common way of splitting the Hamiltonian, without external influence, is in the kinetic energy of the nuclei ( $\hat{T}_N$ ) and the electrons ( $\hat{T}_e$ ), and the potential energy of the nuclear-nuclear repulsion ( $\hat{V}_{NN}$ ), the electron-electron repulsion ( $\hat{V}_{ee}$ ) and the electron-nuclear attraction ( $\hat{V}_{eN}$ ):

$$\hat{H} = \hat{T}_N + \hat{T}_e + \hat{V}_{NN} + \hat{V}_{ee} + \hat{V}_{eN} \quad (1.3)$$

Assuming that the solvent-solute system is one big macro-system, the Hamiltonian describes *all* the interactions. The SE is not solvable for systems larger than one-electron systems, meaning that we need approximations to describe the macro-system at hand. There are usually three steps needed to produce useful theoretical models for such a system.

- First; we need to reduce the macro-system into subsystems. This results in the ability to describe the different subsystems at different level of theory. Usually this is done by describing the molecule with Quantum Mechanics (QMs) and the solvent with Molecular Mechanics (MMs) or Polarizable Continuum model (PCM).
- Second; we need to approximate the SE equation of the subsystem of interest. In this thesis this is done by the Hartree-Fock (HF) method and Density Functional Theory (DFT).
- Third; we need to approximate the mathematical solutions of the model. In chemistry this is usually done by Gaussian-Type Orbitals (GTOs) bases. The method used in this thesis is however Multiresolution Analysis (MRA) through a MultiWavelet (MW) basis



## 1.3 Structure

The structure of this thesis is basically the opposite of the three steps described above. We start off with a discussion about basis sets in chapter 2. The types of bases discussed are the MWs and the atom centered GTO. Chapter 2 is needed to present the different computational methods discussed in chapter 3. The methods discussed are the HF method and DFT. Chapter 4 discusses the inclusion of solvent effect with focus on the Gaussian type formalism. Chapter 5 discusses how the solvent effects are formulated and implemented for the MW basis used in MRChem [1]. Finally, in chapter 6 some results are posted. It contains energy calculations from MRChem compared with Gaussian [2], verifications that the algorithms discussed work and concluding remarks concerning the implementations done in relation to this thesis.



# Chapter 2

## Basis sets

### Contents

---

<b>2.1</b>	<b>Introduction to function basis . . . . .</b>	<b>12</b>
<b>2.2</b>	<b>Atom-centered basis functions . . . . .</b>	<b>12</b>
2.2.1	Gaussian Type Orbitals (GTOs) . . . . .	14
2.2.2	Gaussian contractions . . . . .	15
<b>2.3</b>	<b>MultiResolution Analysis (MRA) . . . . .</b>	<b>16</b>
2.3.1	The Haar basis . . . . .	16
2.3.2	The multiwavelet basis . . . . .	22
<b>2.4</b>	<b>Multiwavelet vs. Gaussian Type Orbitals . . . . .</b>	<b>24</b>

---

Some Partial Differential Equations (PDEs) do not have a known analytical solution, but with approximations and computational tools we can get very close to a solution. This chapter will discuss a few ways of representing functions so that a solution to the PDEs may be approximated. The two most prominent ways of solving PDEs, are either by numerical methods or spectral methods. Finite difference method is one of the most widespread numerical methods (see [3] for further reading). The method transforms the PDE into a set of solvable difference equations. This chapter will, however, focus on the spectral methods used in computational chemistry.

Spectral methods are techniques where one projects the problem onto a set of known basis functions with known properties. By fitting the coefficients to the differential equation at hand, a solution can be obtained. How these basis functions are built to fit the PDEs is the topic of this chapter. The most widespread basis for molecular computations are Atomic Orbital (AO) represented as a linear combination of atom-centered Gaussian functions. Gaussian basis will be discussed in detail, furthermore, the MultiWavelet (MW)

basis will be discussed. MW bases are emerging as a promising alternative to the Gaussian basis and is the basis used for a new way of calculating solvent effects which has been implemented for this thesis.

## 2.1 Introduction to function basis

A basis, from a mathematical point of view, can be something as simple as the vector space  $V = \{\vec{e}_1, \vec{e}_2, \vec{e}_3\} = \{(1, 0, 0), (0, 1, 0), (0, 0, 1)\}$  which spans  $\mathbb{R}^3$ . Any point in space can be written as a linear combination of the three orthonormal vectors, ex:  $(0, 1, 2) = 0\vec{e}_1 + \vec{e}_2 + 2\vec{e}_3$ . This means that any set of vectors  $\{\vec{e}_1, \vec{e}_2, \dots, \vec{e}_n\}$  where  $\langle \vec{e}_i | \vec{e}_j \rangle = \delta_{ij}$ , spans an n-dimensional space.

The same basic principle applies to a basis set of functions, where one represents a function  $f(x)$  as a linear combination of basis functions  $g_\mu(x)$ :

$$f(x) = \sum_{\mu}^n c_{\mu} g_{\mu}(x) \quad (2.1)$$

where, by carefully choosing the basis function  $g_\mu(x)$  and with a large enough  $n$ , one can represent a function accurately. To represent a function accurately is usually not doable because of the complexity of the functions used for quantum molecular calculations. This leads to a choice between accurate representation and reasonable computational time.

- greater number of basis functions  $\implies$  higher accuracy.
- lower number of basis functions  $\implies$  faster calculation.

For computational purposes, the most important factor is that the basis functions have known properties, with differentiation and integration as their main properties for solving differential equations. Another important factor is that the basis set needs to have the possibility to be systematically improved. Meaning that the basis sets should be able to not only be adjusted according to the users preferences but be applicable for the growing computational power emerging every year (Moore's Law [4]).

## 2.2 Atom-centered basis functions

Gaussian-Type Functions (GTFs) and Slater-Type Functions (STFs) are atomic centered functions made to mimic the solutions to the one-electron Schrödinger Equation (SE). Both GTFs and STFs are routinely used as basis functions in computational chemistry.

The STF and GTF are written in equation 2.2 and 2.3. STF represents the cusp of the electronic wave-function well and decays towards 0 at the correct rate.

$$s(r, \theta, \phi; n, l, m, \zeta) = r^{n-l-1} e^{-\zeta r} \Upsilon_{lm}(\vec{r}) = r^{n-1} e^{-\zeta r} Y_{lm}(\theta, \phi) \quad (2.2)$$

A single GTF does not represent the cusp in a correct manner and decays towards 0 too fast. In spite of that, it will after this section become apparent why the GTFs are the more widely used basis functions.

$$g(r, \theta, \phi; n, l, m, \alpha) = r^{2(n-l-1)} e^{-\alpha r^2} \Upsilon_{lm}(\vec{r}) = r^{2n-l-2} e^{-\alpha r^2} Y_{lm}(\theta, \phi) \quad (2.3)$$

In equation 2.2 and 2.3  $r, \theta, \phi$  are the spherical coordinates ( $r = |r - r'|$ ; distance from nuclei),  $n \in \mathbb{Z}$ ,  $l$  and  $m$  are the quantum numbers.  $\zeta$  and  $\alpha$  are positive fitted parameters to the specific GTF or STF,  $\Upsilon_{lm}(\vec{r})$  is related to the spherical harmonics through  $\Upsilon_{lm}(\vec{r}) = r^l Y_{lm}(\theta, \phi)$ . The spherical harmonics are the set of functions that satisfies the angular part of the Laplace equation

$$\nabla^2 Y_{l,m}(\phi, \theta) = 0 \quad (2.4)$$

Using the STF as a basis for chemical calculations is a sound strategy, for the simple reason that the functions can be advocated by the physics of AOs. However, STF poses a problem when it comes to integral evaluation, and especially the three- and four-centered two-electron integrals (2.5) performed in the Hartree-Fock (HF) calculations in the form:

$$g_{pqrs} = \int \int \phi_p(r_1) \phi_q(r_1) \frac{1}{\|r_1 - r_2\|} \phi_r(r_2) \phi_s(r_2) dr_1 dr_2 \quad (2.5)$$

There exists no analytical solution to the two-electron integrals with STF, resulting in time consuming numerical evaluations. In addition, the STF first derivative is not continuous, which causes troublesome evaluation of derivatives.

The only major difference between STF and GTF is that while STFs are linear in the exponent, GTFs are quadratic (Gaussian). The important similarities between a linear and quadratic exponent is that they both decay towards 0 at great distance from the nuclei.

Separability is an important factor. GTFs can be separated into a product of functions, one for each Cartesian direction ( $e^{x^2+y^2+z^2} = e^{x^2} e^{y^2} e^{z^2}$ ). However, integral evaluation is the determining factor in choosing GTFs as building blocks for a basis. Depending on the operator  $\hat{O}$  in  $\langle \chi_\mu | \hat{O} | \chi_\nu \rangle$ , integral evaluation of  $\exp(-x^2)$  can be performed analytically ( $\int_{-\infty}^{\infty} \exp(-\alpha r^2) dr = (\frac{\pi}{\alpha})^{1/2}$ ). This makes sums of GTFs a more efficient representation of AOs, which again translates to a more efficient representation of Molecular Orbitals (MOs).

### 2.2.1 Gaussian Type Orbitals (GTOs)

Equation 2.2 and 2.3 show that the only difference between the two is the radial function; this will be the primary focus. For all types of function bases, the spherical harmonics  $Y_{lm}(\theta, \phi)$  are the same set of functions [5], while the radial part is different. For Gaussian-Type Orbitals (GTOs), the standard form of the radial function

$$g(x, y, z; l, m, n, \alpha) = Nx^l y^m z^n e^{-\alpha r^2} \quad (2.6)$$

is relatively straightforward, with a few key properties. If the sum of the parameters  $l$ ,  $m$  and  $n$  are equal to 0, the function does not contain any radial nodes. This means that a sum of functions with  $L = l + m + n = 0$  can be fitted to represent a 1s GTO. With this logic, it is theoretically possible to build all kinds of AOs from the universal GTO by varying the angular momentum quantum number  $L$ , the normalization  $N$  and the parameter  $\alpha$ .

- 1s

$$g_{1s} = Ne^{-\alpha r^2} \quad (2.7)$$

- 2p

$$\begin{aligned} g_{2p_x} &= Nx e^{-\alpha r^2} \\ g_{2p_y} &= Ny e^{-\alpha r^2} \\ g_{2p_z} &= Nz e^{-\alpha r^2} \end{aligned} \quad (2.8)$$

- 3d

$$\begin{aligned} g_{2d_{xx}} &= Nx^2 e^{-\alpha r^2} \\ g_{2d_{xy}} &= Nxy e^{-\alpha r^2} \\ g_{2d_{xz}} &= Nxz e^{-\alpha r^2} \\ g_{2d_{yy}} &= Ny^2 e^{-\alpha r^2} \\ g_{2d_{yz}} &= Nyz e^{-\alpha r^2} \\ g_{2d_{zz}} &= Nz^2 e^{-\alpha r^2} \end{aligned} \quad (2.9)$$

This way of building the orbital can be continued for 4f, 5g etc, the building blocks are often referred to as primitives or Gaussian primitives. At first glance these functions have a few quirks: The primitives are not eigenfunctions of the square angular momentum operator ( $\hat{L}^2$ ), and there are

too many  $d$  orbitals and consequently too many  $f$  and  $g$  orbitals. Although this seems odd, it is not a problem, rather a clever design, superposing three  $d$ -orbitals gives one totally symmetric  $s$ -orbital;

$$g_{d_{xx}} + g_{d_{yy}} + g_{d_{zz}} = g_s \quad (2.10)$$

$$N_1 x^2 e^{-\alpha r^2} + N_2 y^2 e^{-\alpha r^2} + N_3 z^2 e^{-\alpha r^2} = N' r^2 e^{-\alpha r^2} \quad (2.11)$$

where  $r^2 = x^2 + y^2 + z^2$

### 2.2.2 Gaussian contractions

It is important to note that a single Gaussian primitive in itself is *usually* not used to mimic the solutions of the one-electron SE. However, superposing a collection of primitives can be used to mimic the one electron-system. These collections are typically called contractions, and are a collection of primitives with the same total angular momentum  $L$  but with different  $\alpha$ . The  $\alpha$ 's are typically fitted from quantum calculations (HF, post HF).

This means that the more primitives and the better fitted the  $\alpha$  parameter is, the more accuracy can be expected from the basis-set. This makes the two goals of a function-basis-set posted in the introduction of this chapter a reality; systematic improvement of the basis set and the connection to the physical world.

Doing this contraction lowers the cost of computations, and we get a more physically sound function. Still, for high accuracy calculations, the uncontracted versions are used. The design of the basis sets usually has contracted functions to represent core orbitals and uncontracted bases for the valence orbitals. This gives a more accurate representation of the chemically important valence electrons, while the core electrons, which are usually not part of a chemical bond, are more fixed in space.

An important notion on Gaussian basis sets is that since there are many ways of choosing the  $\alpha$  parameters and many ways to contract the Gaussian primitives, there are a lot of different Gaussian basis sets in use and in development. This is a two sided issue. On the one hand, the user can use a basis set that is close to perfect for the system and the properties that are in question. On the other hand, knowing which basis-set is the best is difficult for inexperienced users.

Another issue is that when more accurate basis sets are developed, which in many cases means more basis functions, the linear dependency in the functions starts to play a big role. The linear dependency leads to a loss of accuracy, due to numerical instabilities, if the number of functions are

too large. This means that there is a limit to how accurate calculations can become with GTO.

Although GTOs have problems achieving chemical accuracy ( $\sim 1\text{kcal/mol}$ ) and the limitations of what the GTO can achieve are closing in, the basis sets are widely used and new basis-sets are being produced [6]. A promising new type of basis-functions is the MW basis functions, which will be in focus in the next section.

## 2.3 MultiResolution Analysis (MRA)

Multiresolution Analysis (MRA) is a different approach to the representation of functions for computational chemistry purposes. The main upside of using MRA is that in some resolution differs for different parts of the space you are working in. This means that starting from an analytical function, say  $\exp(-|r|)$ , one can take the function and project it onto a grid where there are more data-points around  $r = 0$  and less as we approach larger displacements. With the adaptive grid structure of the MRA, one could argue that the MW bases can be classified as somewhere in between a numerical method and a spectral method.

The following discussion will limit us to a 1-dimensional unit interval and not the whole  $\mathbb{R}$ . But before discussing the multi-wavelet basis, it is useful to discuss a slightly simpler basis that, in principle, has the same build and exhibits many of the same properties: the Haar-basis[7].

### 2.3.1 The Haar basis

The Haar basis was defined by Alfred Haar[7]. It is one of the first MRA bases and is used in this thesis as an introduction to MRA for the simple reason that the equations are simpler which makes the deduction simpler to read.

#### The build

The Haar basis in  $L^2[0, 1]$  is the collection of functions with a specific property (2.12)

$$\chi_l^n(x) = 2^{n/2}\chi(2x^n - l) \quad (2.12)$$

With  $n, l \in \mathbb{Z}$  and by varying  $n$  and  $l$  one changes the domain of the function. In MRA,  $\chi$  is commonly known as the scaling function, in the Haar basis it



is defined as

$$\chi_0^0(x) = \begin{cases} 1 & \text{for } x \in [0, 1) \\ 0 & \text{else} \end{cases} \quad (2.13)$$

which is a very simple function, but exhibits the property in equation 2.12 which makes it the simplest possible basis for a complete MRA basis. It is important to note the two scale difference equation (2.14):

$$\chi(x) = \chi(2x) + \chi(2x - 1) \quad (2.14)$$

$$\chi_l^n(x) = \chi_{2l}^{n+1}(2^{n+1}x - 2l) + \chi_{2l+1}^{n+1}(2^{n+1}x - 2l - 1) \quad (2.15)$$

which is resulting from 2.13 and 2.12.

Introducing another function with many of the same properties, the Haar function

$$h_l^n(x) = 2^{n/2}h(2^n x - l) \quad (2.16)$$

where  $n, l \in \mathbb{Z}$ .

$$h_0^0(x) = \begin{cases} 1 & \text{for } x \in [0, 1/2) \\ -1 & \text{for } x \in [1/2, 1) \\ 0 & \text{else} \end{cases} \quad (2.17)$$

Although the Scaling functions may be used as basis functions, it is not generally the case, and the set of the Haar functions and scaling functions is used. The Haar functions  $h$  and the scaling functions  $\chi$  are connected via another very important two scale relation:

$$h(x) = \chi(2x) - \chi(2x - 1) \quad (2.18)$$

$$h_l^n(x) = \chi_{2l}^{n+1}(2^{n+1}x - 2l) - \chi_{2l+1}^{n+1}(2^{n+1}x - 2l - 1) \quad (2.19)$$

From the definitions above, the Haar-functions  $h(x)$  and the scaling functions  $\chi(x)$  have a few key properties which make the collection of the two better suited as a basis:

- Their  $L^2$ -norm is equal to 1 for all  $n, l \in \mathbb{Z}$

$$\int_{\mathbb{R}} h_l^n(x)^2 dx = \int_{\mathbb{R}} \chi_l^n(x)^2 dx = 1 \quad (2.20)$$

- The Haar functions are orthonormal in  $L^2[0, 1]$

$$\langle h_l^n, h_{l'}^{n'} \rangle = \int h_l^n(x) h_{l'}^{n'}(x) dx = \delta_{n,n'} \delta_{l,l'} \text{ for } n, n', l, l' \in \mathbb{Z} \quad (2.21)$$

- The Haar functions are dense in  $L^2[0, 1]$ , meaning that they produce a basis that is arbitrary close to  $L^2[0, 1]$ . This is a consequence of the fact that any continuous function ( $C[0, 1]$ ) can be approximated with arbitrary precision by the Haar Functions with sufficiently small dyadic interval.

The functions  $\chi_l^n(x)$  defined on  $[0, 1]$  create a hierarchical chain of linear subspaces in  $L^2[0, 1]$ :

$$V^0 \subset V^1 \subset \dots \subset V^{n-1} \subset V^n \subset V^{n+1} \subset \dots \subset L^2[0, 1] \quad (2.22)$$

where  $V^0$  is spanned by the single function  $\chi_0^0$ ,  $V^1$  spanned by  $\{\chi_0^1, \chi_1^1\}$ . Any space  $V^n$  is then defined as being spanned by:  $\sum_l \chi_l^n$

For an equivalent representation, we produce a space  $W^n$  called Difference space, defined as  $V^{n+1} = W^n \oplus V^n$  where the Haar functions span  $W^n$ .

Applying the definition of  $W^n$  recursively leads to equation (2.23)

$$V^n = V^0 \oplus W^0 \oplus W^1 \oplus \dots \oplus W^{n-1} \quad (2.23)$$

### Projecting functions

The next step is to determine the scaling and difference coefficients of a projection of a function  $f(x)$ . The function  $f(x)$  is defined as values of scaled averages of  $f(x)$  in intervals of length  $2^{-j}$

$$s_l^j = \int_{\mathbb{R}} \chi_j^l(x) f(x) dx = 2^{j/2} \int_{2^{-j}l}^{2^{-j}(l+1)} f(x) dx \quad (2.24)$$

Using the two-scale difference equations, we obtain:

$$\begin{aligned} d_l^{j-1} &= \int_{\mathbb{R}} h_l^{j-1}(x) f(x) dx = 2^{(j-1)/2} \int h(2^{(j-1)}x - l) f(x) dx \\ d_l^{j-1} &= 2^{(j-1)/2} \left( \int \chi(2^j x - 2l) f(x) dx - \int \chi(2^j x - 2l - 1) f(x) dx \right) \\ d_l^{j-1} &= 2^{(j-1)/2} \left( \int_{2^{-j}(2l)}^{2^{-j}(2l+1)} f(x) dx - \int_{2^{-j}(2l+1)}^{2^{-j}(2l+2)} f(x) dx \right) \\ d_l^{j-1} &= 2^{-1/2} (s_{2l}^j - s_{2l+1}^j) \end{aligned} \quad (2.25)$$

where  $d$  is called the difference coefficients, the coefficient for the Haar functions  $h$ ,

$$\begin{aligned}
s_l^{j-1} &= \int_{\mathbb{R}} \chi_l^{j-1}(x) f(x) dx = 2^{(j-1)/2} \int h(2^{(j-1)}x - l) f(x) dx \\
s_l^j &= 2^{(j-1)/2} \left( \int \chi(2^j x - 2l) f(x) dx + \int \chi(2^j x - 2l - 1) f(x) dx \right) \\
s_l^j &= 2^{(j-1)/2} \left( \int_{2^{-j}(2l)}^{2^{-j}(2l+1)} f(x) dx + \int_{2^{-j}(2l+1)}^{2^{-j}(2l+2)} f(x) dx \right) \\
s_l^{j-1} &= 2^{-1/2} (s_{2l}^j + s_{2l+1}^j)
\end{aligned} \tag{2.26}$$

where  $s$  is called the scaling coefficients. With this we have a method of obtaining the Haar/difference coefficients (2.25) and scaling coefficients (2.26). An important notion is that the projection of coefficients to a coarser scale can be written as:

$$\begin{pmatrix} d_l^n \\ s_l^n \end{pmatrix} = \begin{pmatrix} 2^{-1/2} & -2^{-1/2} \\ 2^{-1/2} & 2^{-1/2} \end{pmatrix} \begin{pmatrix} s_{2n}^{j+1} \\ s_{2n+1}^{j+1} \end{pmatrix} \tag{2.27}$$

And the invers:

$$\begin{pmatrix} s_{2n}^{j+1} \\ s_{2n+1}^{j+1} \end{pmatrix} = \begin{pmatrix} 2^{-1/2} & 2^{-1/2} \\ -2^{-1/2} & 2^{-1/2} \end{pmatrix} \begin{pmatrix} d_l^n \\ s_l^n \end{pmatrix} \tag{2.28}$$

It is now possible to evaluate the entire set of coefficients.

### Example

The main purpose of the MRA bases is that the difference coefficients will be small for smooth functions. To illustrate the effect, an example program was made using MATHEMATICA[8]. The example program projects the function  $f(x)$  onto a Haar basis at scale 4.

$$f(x) = e^{-100(x-0.5)^2} \tag{2.29}$$

The function is then approximated according to definition 2.23

$$f^5(x) \approx \sum_l^{2^n-1} \sum_n^5 s_l^n \chi_l^n = s_0^0 \chi_0^0 + \sum_l^{2^n-1} \sum_n^4 d_l^n h_l^n \tag{2.30}$$

With scaling and difference coefficients calculated with the relationship 2.27

The figures in 2.2 shows five functions, summing up the first five results in the sixth figure. Note that the functions are on a uniform grid in every

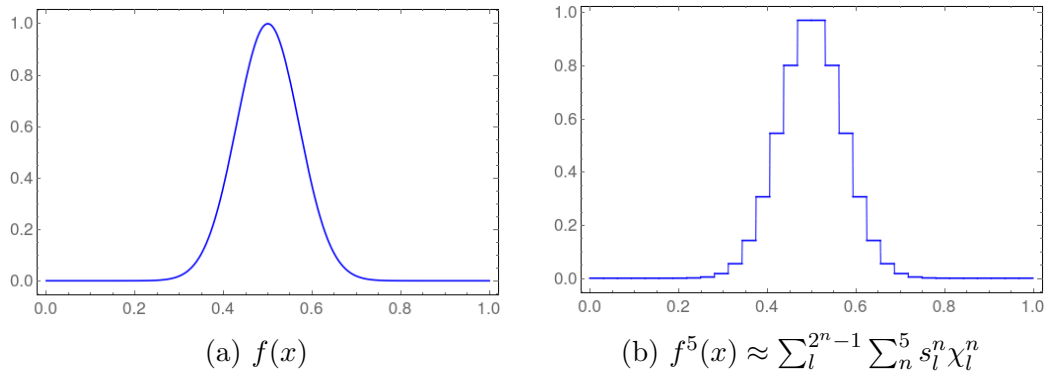


Figure 2.1: The projected function  $f^5(x)$  and the original function  $f(x)$ , plotted with MATHEMATICA

figure, this is to illustrate the effect of adaptivity. The example shows that the coefficients of the Haar functions, in regions where the approximation of the function is good from the sum of the coarser scales, are closing in on 0. This means that in these regions (see figure 2.2c in region  $(0,0.2)$  and  $(0.8,1)$ ) the refinement of the grid can be stopped. In other regions (around 0.4 and 0.6) the refinement continues, this is how an adaptive grid is made. Although the functions can be more complicated and the basis functions more complicated, the principle of MRA is the same.

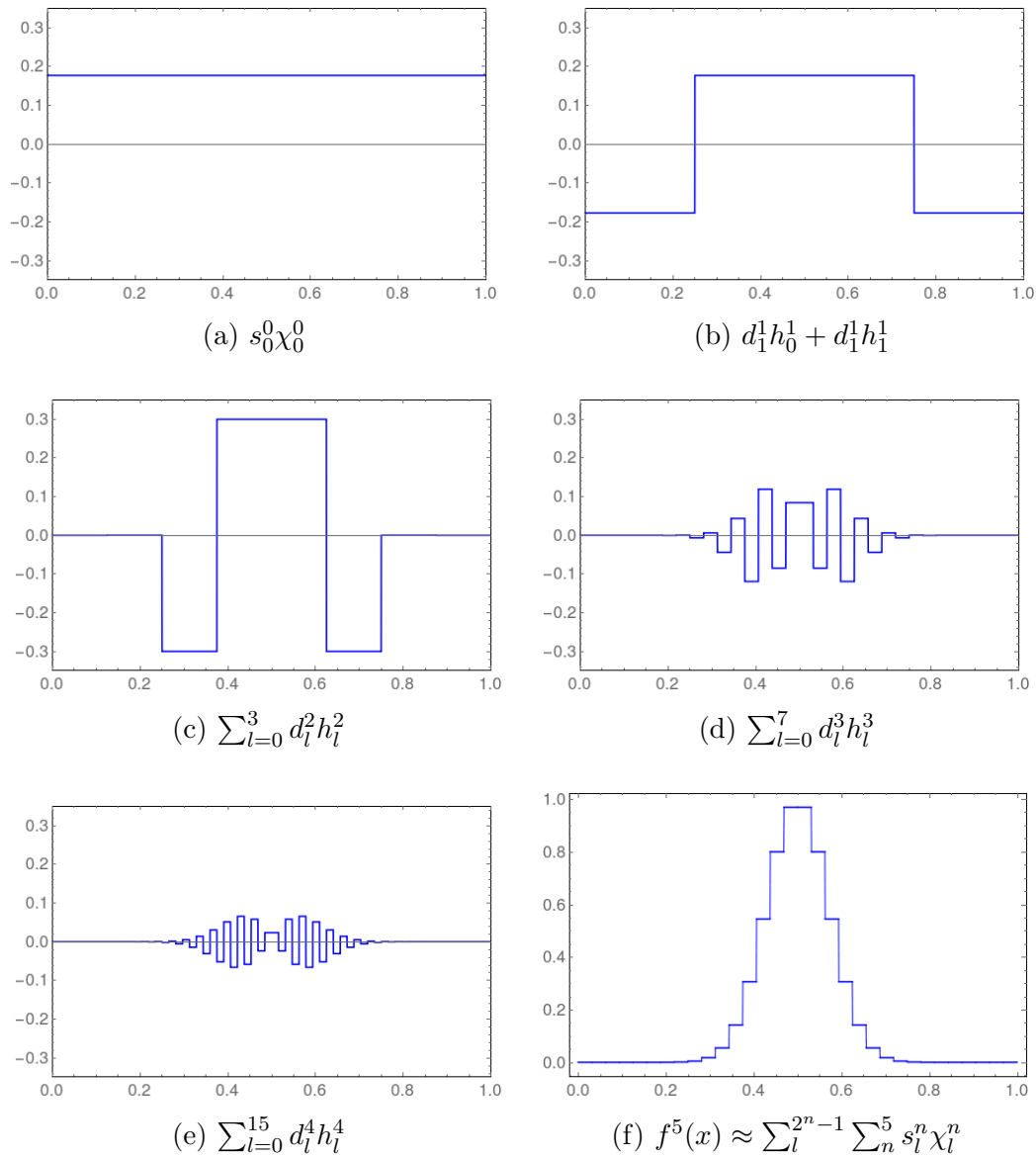


Figure 2.2: The road to approximation, plotted with MATHEMATICA

### 2.3.2 The multiwavelet basis

The similarities between the MW basis and the Haar basis is profound. In simple terms, the Haar functions and the scaling functions are replaced by polynomial bases. This means that the Haar basis is a multiwavelet basis with polynomial order 0.

There are a few important properties that emerge when higher order polynomials are used, but first we need to discuss the build.

#### The build

Building the multiwavelet basis is very similar to the Haar basis. The scaling function for the multiwavelet basis (2.31) is built in a similar manner as for the Haar basis (2.12) and the wavelet functions (2.32) are constructed in a similar manner as the Haar function for the Haar basis (2.16). They produce the same sequence of subspaces as in 2.22 and exhibit the same properties as in 2.23.

The big difference is the two scale relations:

$$\phi_{i,l}^n(x) = \sqrt{2} \sum_{j=0}^k (\mathbf{H}_{ij}^{(0)} \phi_{j,2l}^{n+1}(x) + \mathbf{H}_{ij}^{(1)} \phi_{j,2l+1}^{n+1}(x)) \quad (2.31)$$

$$\psi_{i,l}^n(x) = \sqrt{2} \sum_{j=0}^k (\mathbf{G}_{ij}^{(0)} \phi_{j,2l}^{n+1}(x) + \mathbf{G}_{ij}^{(1)} \phi_{j,2l+1}^{n+1}(x)) \quad (2.32)$$

Since the functions now are polynomials, we get the  $H^{(m)}$  matrices and the  $G^{(m)}$  matrices instead of the simpler two-scale relations for the Haar-basis (2.14 and 2.18). The matrices describe the transformation between different spaces.

The disjoint form of the wavelets  $\psi$  and scaling functions  $\phi$  means that there is an overlap and that the relation between two scales is made up of a matrix of matrices  $(G^{(1)}, G^{(0)}, H^{(1)}, H^{(0)})$ , with the representation of  $\psi$  and  $\phi$  as vectors  $\vec{\psi}$  and  $\vec{\phi}$

$$\begin{pmatrix} \vec{\psi}_l^n \\ \vec{\phi}_l^n \end{pmatrix} = \begin{pmatrix} G^{(1)} & G^{(0)} \\ H^{(1)} & H^{(0)} \end{pmatrix} \begin{pmatrix} \vec{\psi}_{2l+1}^{n+1} \\ \vec{\phi}_{2l}^{n+1} \end{pmatrix} \quad (2.33)$$

### Projecting Functions

Projecting a function on the scaling space  $V_k^n$  where  $k$  is the highest order of polynomial is done in a similar manner as for the Haar basis. The MW transform:

$$f(x) \approx P_k^n f(x) = f^n(x) = \sum_{l=0}^{2^n-1} \sum_{j=0}^k s_{j,l}^{n,f} \phi_{j,l}^n(x) \quad (2.34)$$

where  $n$  is the scale on which  $f$  is projected,  $l$  is the individual function for each box,  $j$  the order of the polynomial and  $s_{j,l}^{n,f}$  is defined as in equation 2.35 (see eq. 2.26)

$$s_{j,l}^{n,f} = \int_0^1 \phi_{j,l}^n(x) f(x) dx \quad (2.35)$$

### The Poisson and Helmholtz operator

Derivative operators, and in particular the Laplacian ( $\nabla^2$ ), poses a problem in the MW basis. The reason for this is the discontinuity in the basis. One way to solve this is by transforming the differential equation into an integral equation.

The numerical noise due to the discontinuity, here represented as a wave, amplifies when the Laplacian is applied:

$$\nabla^2(f(x) + \lambda e^{ikx}) = f''(x) - k^2 \lambda e^{ikx} \quad (2.36)$$

where  $\lambda$  is the order of noise and  $k$  the frequency. The inverse operator, however, has the opposite effect:

$$(\nabla^2)^{-1}(f(x) + \lambda e^{ikx}) = (\nabla^2)^{-1}f(x) - \frac{\lambda}{k^2} e^{ikx} \quad (2.37)$$

This means that two convolution operators are introduced, the Poisson ( $\hat{\mathcal{P}}$ ) and Helmholtz ( $\hat{\mathcal{H}}^\nu$ ) operator. The Poisson operator

$$\hat{\mathcal{P}}[f](r) = \int \frac{1}{4\pi||r - r'||} f(r') dr' \quad (2.38)$$

is the inverse Laplacian ( $\hat{\mathcal{P}} = (-\nabla^2)^{-1}$ ) and the Helmholtz operator

$$\hat{\mathcal{H}}^\nu[f](r) = \int \frac{e^{-\nu||r-r'||}}{4\pi||r - r'||} f(r') dr' \quad (2.39)$$

is the inverse of the shifted Laplacian ( $\hat{\mathcal{H}}^\nu = (-\nabla^2 + \nu^2)^{-1}$ ). Both convolution operators have been implemented in MRChem [1], and used in this thesis for solving the equations emerging from chapter 3, 4 and 5.

## 2.4 Multiwavelet vs. Gaussian Type Orbitals

There are many differences between GTO and multiwavelets. This section will discuss the most important differences.

- The Gaussian basis has issues when it comes to reliably determining how accurate the calculations are with a given method. This is on the other hand something the MW codes do perfectly.
- The scaling of computational time vs. system size for a naive HF calculation with GTO is  $n^4$  where  $n$  is the number of orbitals, this is, after decades of optimization closer to  $n$  with small and localized Gaussian basis sets.[9] With the MW basis, the scaling is quadratic due to the inherent linear scaling of the necessary integral convolution operators ( $\hat{\mathcal{P}}$  and  $\hat{\mathcal{H}}^\nu$ ) [10]. However, the MW computations come with a larger prefactor.
- The two-electron integrals (2.5) pose a problem for both the MW and GTO codes. Although the gaussian form of the basis functions in GTO has an analytic form, the two-electron integrals pose a numerical problem. This problem is however simpler in the MW codes, but to represent a function in MW one typically needs more functions. If the Gaussian approach uses 1'000 basis functions, the MW basis needs, depending on the order of polynomials, somewhere between  $10^6$  and  $10^7$  functions to obtain the same accuracy.
- With the simplicity of the MW in mind, it is safe to assume that the possibility of parallelization is greater for the MW codes. The MADNESS code written at Stony Brook University in New York is leading the parallelization effort for chemical computations on MW [11].
- Some properties like magnetizability and NMR-shielding are affected by the gauge origin. This means that basis functions that have a specific origin, like GTOs, have issues. There have been many attempts to solve this problem with the GTO. Many of them are successful, and especially the Gauge Including Atomic Orbitals (GIAO) [12]. Because of the highly adaptable grid and the theoretical completeness of the MW basis, this problem is not an issue and successful implementations have been produced for calculating NMR-shielding constant and magnetizabilities in MRCHEM [13].



# Chapter 3

## QM-methods

### Contents

---

<b>3.1</b>	<b>The electronic Schrödinger equation . . . . .</b>	<b>26</b>
<b>3.2</b>	<b>The Hartree-Fock method . . . . .</b>	<b>27</b>
3.2.1	General considerations . . . . .	27
3.2.2	Hartree-Fock method with Gaussian Type Orbitals	30
3.2.3	Hartree-Fock method with multi-wavelets . . . . .	31
<b>3.3</b>	<b>Density Functional Theory . . . . .</b>	<b>32</b>
<b>3.4</b>	<b>Energy calculation with multi-wavelets . . . . .</b>	<b>34</b>
3.4.1	Energy calculations for Hartree-Fock . . . . .	34
3.4.2	Energy calculations for Density Functional Theory	35

---

This chapter contains an outline of the Hartree-Fock (HF) method and Density Functional Theory (DFT). The focus will mainly be on the HF Self-Consistent Field (SCF) method, HF method for short, which is one of the big driving forces behind modern computational chemistry. The HF method is important not only in its own right, but is used as a starting point for other more accurate models for computing electronic structures in molecules. (Couple-Cluster (CC), Møller-Plesset perturbation (MPn) and more are based on HF [14]). The derivation of the HF method follows that of standard textbooks like Atkins [5], Szabo and Ostlund [15], Helgaker [14] and F. Jensen [16] and from the thesis of S.R. Jensen [17]

### 3.1 The electronic Schrödinger equation

As a starting point for the discussion one can use the non-relativistic Hamiltonian from equation 1.3, written again in 3.1

$$\hat{H} = \hat{T}_N + \hat{T}_e + \hat{V}_{NN} + \hat{V}_{ee} + \hat{V}_{eN} \quad (3.1)$$

The most widespread first step approximation is the Born-Oppenheimer approximation (BO). The BO views the nuclei as fixed in space and the electrons as particles in a static potential field made by the nuclei. The motivation for this is that the electrons are much lighter than protons and neutrons ( $1836.1493m_e$  and  $1838.6802m_e$  [18]). This leads to the following assumption; the electrons instantly react to the motion of the nuclei, which leads to; in an electronic time scale, the nuclei are fixed in space. Since the nuclei are fixed in space, the instantaneous correlation between the nuclei and electrons can be disregarded and we can separate the nuclear kinetic energy from the Hamiltonian:

$$\hat{H} = \hat{T}_{nuc} + \hat{H}_{el} \quad (3.2)$$

The total electronic Hamiltonian ( $\hat{H}_{el}$ ) consists of four operators, the electron kinetic energy

$$\hat{T}_e = - \sum_i \frac{1}{2} \nabla_i^2 \quad (3.3)$$

the electron-nuclei attraction

$$\hat{V}_{eN} = - \sum_{i,I} \frac{Z_I}{||r_i - R_I||} \quad (3.4)$$

the electron-electron repulsion

$$\hat{V}_{ee} = - \sum_{i=1} \sum_{i>j} \frac{1}{||r_i - r_j||} \quad (3.5)$$

and the nuclear-nuclear repulsion

$$\hat{V}_{NN} = \sum_{I>J} \frac{Z_I Z_J}{||R_I - R_J||} \quad (3.6)$$

What is left is the dilemma of solving the electronic Schrödinger Equation (SE);

$$\hat{H}_{el} \Psi_{el} = E_{el} \Psi_{el}. \quad (3.7)$$

which, for the remainder of this chapter, will be the main equation, making the subscript *el* redundant.

There is a particular state of a quantum-chemical system called ground state ( $\psi_0$ ).  $\psi_0$  is associated via the SE to its eigenvalue  $E_0$ , which is called ground state energy (the minimal energy of a system). This state is of special importance to computational chemists. Under normal lab-conditions this is the state which is most populated, which means that many chemical properties can be explained from the ground state system. This means that making adequate approximations to the ground state wave-function has been given a lot of attention through the development of Quantum Mechanic (QM) methods. The way the ground state system can be calculated is by the use of the variational principle, which states that for any given  $\hat{H}$ , with a true ground state  $\psi_0$ , we have for an arbitrary approximated wave-function  $\tilde{\psi}$

$$\frac{\langle \tilde{\psi} | \hat{H} | \tilde{\psi} \rangle}{\langle \tilde{\psi} | \tilde{\psi} \rangle} \geq \frac{\langle \psi_0 | \hat{H} | \psi_0 \rangle}{\langle \psi_0 | \psi_0 \rangle} \quad (3.8)$$

which has an expectation value that is always greater or equal to the true ground state. This theorem results in the possibility of formulating methods as a minimization problem. The variational formulation is an important part of both the HF method and DFT.

## 3.2 The Hartree-Fock method

The HF method is formulated differently with respect to which basis is used. In this thesis the Gaussian-Type Orbital (GTO) and the MultiWavelet (MW) basis have been considered and will therefore be considered again in relation to HF. First some general considerations will be presented, then the two bases force a split in the section for which the formulation differs.

### 3.2.1 General considerations

One of the major problems of solving the electronic-SE is the high dimensionality that emerges when working with molecules. The dimensionality of a system with  $n$  electrons results in a wave-function as a  $3n$ -dimensional scalar function (disregarding spin). This is not feasible for computational purposes, we introduce  $\Psi$  as a product of  $n$  one-electron wave-functions called spin-orbitals ( $\phi_i$ ).

$$\Psi(\vec{x}_1, \vec{x}_2, \vec{x}_3, \dots, \vec{x}_N) = \sum_m c_m \phi_1^m(\vec{x}_1) \phi_2^m(\vec{x}_2) \phi_3^m(\vec{x}_3), \dots, \phi_n^m(\vec{x}_n), \quad (3.9)$$

The spin-orbitals ( $\phi_i$ ) are solutions of the one-electron SE.

$$\hat{h}_i \phi_i = \left( -\frac{1}{2} \nabla^2 - \sum_I \frac{Z_I}{|r_i - R_I|} \right) \phi_i \quad (3.10)$$

This representation, however, does not converge well and a large number of terms are usually needed and is missing electron-electron repulsion. In addition, the representation does not abide the fermionic properties of the electrons (Pauli exclusion principle[19]). The Pauli-principle states that a fermionic wave function needs to be antisymmetric with respect to exchange of two particles.

$$\Psi(\vec{x}_1, \vec{x}_2, \vec{x}_3, \dots, \vec{x}_n) = -\Psi(\vec{x}_1, \vec{x}_3, \vec{x}_2, \dots, \vec{x}_n) \quad (3.11)$$

Slater-determinants are therefore used:

$$|\phi\rangle = (N!)^{-1/2} \begin{vmatrix} \phi_1(\vec{x}_1) & \phi_1(\vec{x}_2) & \dots & \phi_1(\vec{x}_n) \\ \phi_2(\vec{x}_1) & \phi_2(\vec{x}_2) & \dots & \phi_2(\vec{x}_n) \\ \vdots & \vdots & \ddots & \vdots \\ \phi_{n-1}(\vec{x}_1) & \phi_{n-1}(\vec{x}_2) & \dots & \phi_{n-1}(\vec{x}_n) \\ \phi_n(\vec{x}_1) & \phi_n(\vec{x}_2) & \dots & \phi_n(\vec{x}_n) \end{vmatrix} = |\phi_1 \phi_2 \dots \phi_{n-1} \phi_n\rangle \quad (3.12)$$

The HF method considers a single Slater determinant as the trail wave-function, one of the ways of improving the HF method is by including more determinants.

To derive the HF equations, it is potent to sort the different parts of the Hamiltonian (3.3)(3.5)(3.4)(3.6) after electron indices:

$$\hat{H} = \hat{V}_{NN} + \sum_{i=1} h_i + \sum_{i=1} \sum_{j>i} g_{ij} \quad (3.13)$$

where  $g_{ij} = 1/||r_i - r_j||$ ,  $\hat{V}_{NN}$  is a scalar multiplication operator  $\langle \phi | \hat{V}_{NN} | \phi \rangle = V_{NN} \langle \phi | \phi \rangle$ . The expectation value of  $h_i$  for a specific  $i = k$  is:

$$\langle \phi_1 \phi_2 \dots \phi_k \dots \phi_n | h_k | \phi_1 \phi_2 \dots \phi_k \dots \phi_{n-1} \phi_n \rangle \quad (3.14)$$

$$= \langle \phi_1 | \phi_1 \rangle \langle \phi_2 | \phi_2 \rangle \dots \langle \phi_k | h_k | \phi_k \rangle \dots \langle \phi_n | \phi_n \rangle = \langle \phi_k | h_k | \phi_k \rangle \quad (3.15)$$

The two-electron part of the operator demands the full representation of the Slater determinant. Considering a two-electron system with the short

hand notation  $\vec{x}_i = \{\vec{r}_i, q_i\}$ ,  $q$  is the charge.

$$\langle \phi_1 \phi_2 | g_{12} | \phi_1 \phi_2 \rangle \quad (3.16)$$

$$= \frac{1}{2} \langle \phi_1(\vec{x}_1) \phi_2(\vec{x}_2) - \phi_1(\vec{x}_2) \phi_2(\vec{x}_1) | g_{12} | \phi_1(\vec{x}_1) \phi_2(\vec{x}_2) - \phi_1(\vec{x}_2) \phi_2(\vec{x}_1) \rangle \quad (3.17)$$

$$\begin{aligned} &= \frac{1}{2} \langle \phi_1(\vec{x}_1) \phi_2(\vec{x}_2) | g_{12} | \phi_1(\vec{x}_1) \phi_2(\vec{x}_2) \rangle \\ &+ \frac{1}{2} \langle \phi_1(\vec{x}_2) \phi_2(\vec{x}_1) | g_{12} | \phi_1(\vec{x}_2) \phi_2(\vec{x}_1) \rangle \\ &- \frac{1}{2} \langle \phi_1(\vec{x}_1) \phi_2(\vec{x}_2) | g_{12} | \phi_1(\vec{x}_2) \phi_2(\vec{x}_1) \rangle \\ &- \frac{1}{2} \langle \phi_1(\vec{x}_2) \phi_2(\vec{x}_1) | g_{12} | \phi_1(\vec{x}_1) \phi_2(\vec{x}_2) \rangle \end{aligned} \quad (3.18)$$

where the integrals are over  $\vec{x}_i$ , renaming the indices gives us:

$$\langle \phi_1 \phi_2 | g_{12} | \phi_1 \phi_2 \rangle \quad (3.19)$$

$$= \langle \phi_1(\vec{x}_1) \phi_2(\vec{x}_2) | g_{12} | \phi_1(\vec{x}_1) \phi_2(\vec{x}_2) \rangle \quad (3.20)$$

$$- \langle \phi_1(\vec{x}_2) \phi_2(\vec{x}_1) | g_{12} | \phi_1(\vec{x}_1) \phi_2(\vec{x}_2) \rangle \quad (3.21)$$

$$= \hat{J}_{12} - \hat{K}_{12} \quad (3.22)$$

Note that  $g_{12} = g_{21}$ . This procedure is valid for systems with arbitrary number of electrons.

With this we arrive at the one-orbital Hartree-Fock equation, where the nuclear-nuclear ( $\hat{V}_{NN}$ ) repulsion is omitted,

$$\hat{F} \phi_i = \hat{h}_i \phi_i + \frac{1}{2} \sum_j (\hat{J}_j - \hat{K}_j) \phi_i = \epsilon_i \phi_i \quad (3.23)$$

$\epsilon_i$  is the orbital energy eigenvalue.  $\hat{V}_{ee}$  (3.5) is transformed into the Coulomb interaction  $\hat{J}_j$  and the Exchange operator  $\hat{K}_j$ , which assumes that  $\phi$  is known for the  $j - 1$  other electrons. The 1/2 factor is to correct for the double counting emerging in both  $\hat{J}$  and  $\hat{K}$

$$\hat{J}_j \phi_i(\vec{x}) = \langle \phi_j(\vec{x}') | \frac{1}{\|r - r'\|} | \phi_j(\vec{x}') \rangle \phi_i(\vec{x}) \quad (3.24)$$

$$\hat{K}_j \phi_i(\vec{x}) = \langle \phi_j(\vec{x}') | \frac{1}{\|r - r'\|} | \phi_i(\vec{x}') \rangle \phi_i(\vec{x}) \quad (3.25)$$

The Coulomb operator ( $\hat{J}_j$ ) takes into account the Coulombic repulsion between electrons. The Exchange operator ( $\hat{K}_j$ ) represents the modification of this energy that can be ascribed to the effect of spin correlation.

Equation 3.23 is the same for both the formulation of the method in GTO and MW bases and is in theory ready for implementation. But as the molecules grow, the complexity of the numerical solutions increases and rapidly becomes unfeasible. This is why additional modifications are needed and the modifications differ for the different bases.

### 3.2.2 Hartree-Fock method with Gaussian Type Orbitals

The additional modifications needed to implement the HF method in a GTO basis comes from the Linear Combination of Atomic Orbitals (LCAO) (3.26) which states that one can express a Molecular Orbital (MO) ( $\phi_i$ ) as a linear combination of Atomic Orbitals (AOs) ( $\chi_{\mu i}$ ).

$$\phi_i = \sum_{\mu}^{N_{\mu}} c_{\mu i} \chi_{\mu} \quad (3.26)$$

where  $i$  is the specific MO,  $\mu$  is ranging over the  $N_{\mu}$  basis functions ( $\chi_{\mu}$ ) in use. This procedure is called the LCAO, and was independently developed by C.C.J. Roothaan [20] in 1951 and G.G. Hall [21] in 1950. Assuming that the AOs represented by GTO are known, this transforms the differential equation (3.23) into a problem where one needs to compute the coefficients  $c_{\mu i}$ .

Substituting the expansion from equation 3.26 in equation 3.23 yields:

$$\hat{F} \sum_{\mu}^{N_{\mu}} c_{\mu i} \chi_{\mu}(r_1) = \epsilon_i \sum_{\mu}^{N_{\mu}} c_{\mu i} \chi_{\mu}(r_1) \quad (3.27)$$

Multiplying each side by  $\chi_{\mu'}^*(r_1)$  and integrating over all space gives:

$$\sum_{\mu}^{N_{\mu}} \langle \chi_{\mu'}(r_1) | \hat{F} | \chi_{\mu}(r_1) \rangle = \epsilon_i \sum_{\mu}^{N_{\mu}} \langle \chi_{\mu'}(r_1) | \chi_{\mu}(r_1) \rangle \quad (3.28)$$

Introducing the overlap matrix,  $\mathbf{S}$ , and the Fock matrix,  $\mathbf{F}$ , both with dimensions  $N_{\mu} \times N_{\mu}$  and with matrix elements  $S$  and  $F$ ;

$$S_{\mu' \mu} = \langle \chi_{\mu'}(r_1) | \chi_{\mu}(r_1) \rangle \quad (3.29)$$

$$F_{\mu' \mu} = \langle \chi_{\mu'}(r_1) | \hat{F} | \chi_{\mu}(r_1) \rangle \quad (3.30)$$

which transforms equation 3.27 into:

$$\sum_{\mu}^{N_{\mu}} F_{\mu'\mu} c_{\mu i} = \epsilon_i \sum_{\mu}^{N_{\mu}} S_{\mu'\mu} c_{\mu i} \quad (3.31)$$

Combining the whole set of equations from the Roothaan equations (3.31) results in a matrix representation of the HF equation (3.23)

$$\mathbf{F}^n \mathbf{c} = \epsilon \mathbf{S} \mathbf{c}^{n+1} \quad (3.32)$$

where every member of the equation is an  $N_{\mu} \times N_{\mu}$  matrix,  $\epsilon$  is a diagonal matrix. Note that  $\mathbf{F}$  has the matrix elements  $F_{\mu'\mu}$  (3.30) that is made from the Fock operator (3.23) that contains the coefficients  $c_{\mu i}$ . Solving equation 3.32 is an iterative process, where one starts with an initial guess of what the matrix  $\mathbf{c}^0$  looks like and from that makes the Fock matrix  $\mathbf{F}^0$  which again changes a new matrix  $\mathbf{c}^1$ . This process is often referred to as a self-consistent field method, thereby HF-SCF method. The SCF is said to converge, and thereby stopped, when the  $\epsilon$  from iteration  $n$  is significantly close (user specified) to  $\epsilon$  from iteration  $n + 1$ .

### 3.2.3 Hartree-Fock method with multi-wavelets

To formulate a solution algorithm for the MW basis, it is useful to write the full HF equation (3.23) for electron  $i$ :

$$\left( -\frac{1}{2} \nabla_i^2 + \sum_I \frac{Z_I}{\|r - r'\|} + \sum_j \langle \phi_j | \frac{1}{\|r - r'\|} | \phi_j \rangle - \sum_j \langle \phi_j | \frac{1}{\|r - r'\|} | \phi_i \rangle \right) \phi_i = \epsilon_i \phi_i \quad (3.33)$$

Note that  $\hat{V}_{eN}$  and  $\hat{J}_j$  are scalar multiplication operators, which makes them easier to work with, results in a notation change where  $\hat{V}_{eN}$  is transformed  $v_{eN}$ . This is done to underline the property and simplify the equations.  $\hat{V}_{eN}$  runs over all electrons as well as nuclei,  $v_{eN}$  runs over the nuclei:

$$v_{eN}(r) = \sum_I \frac{Z_I}{\|r - R_I\|} \quad (3.34)$$

and  $J_j$  is changed to

$$v_{el} = \sum_j^{n/2} 2J_j = 2 \sum_j^{n/2} \hat{\mathcal{P}}[\phi_j \phi_j](r) \quad (3.35)$$

$\hat{K}_j$  represented with  $\hat{\mathcal{P}}$

$$\hat{K}_j \phi_i = \hat{\mathcal{P}}[\phi_i \phi_j](r) \phi_i \quad (3.36)$$

where each  $j$  represents a closed shell doubly occupied orbitals. The number of orbitals is therefore half of the number of electrons,  $n/2$ . With this in mind and some rearranging, we end up with the equation

$$\left( -\nabla^2 - 2\epsilon_i \right) \phi_i = -2 \left( v_{eN} + v_{el} - \hat{K}_j \right) \phi_i \quad (3.37)$$

which is a better representation of equation 3.23 for MW purposes.

Applying  $\hat{\mathcal{H}}^\nu$  to 3.37 results in the equation which is solved in MRCHEM is;

$$\phi_i^{n+1}(r) = -2\hat{\mathcal{H}}^\nu [(v_{eN} + v_{el}^n - \hat{K}_j^n) \phi_i^n](r) \quad (3.38)$$

where  $\nu = (-2\epsilon_i^n)^{-1/2}$ . Note again that the both the right hand side and the left hand side are determined by the orbitals, meaning a SCF procedure with  $\hat{K}$  is applied and updated each iteration for each orbital.

### 3.3 Density Functional Theory

The derivation of the DFT method in this section follows that of the European Summerschool in Quantum Chemistry [22] and that of S.R. Jensen [17]. DFT states that the complexity in the SE equation can be reduced by use of a uniquely defined three-dimensional electron density:

$$\rho(r_1) = N \int |\psi(x_1, x_2, \dots, x_n)|^2 ds_1 dx_2 \dots dx_n \quad (3.39)$$

The connection was made by Hohnberg and Kohn in 1964 [23]. It states that a system can be uniquely determined by  $\rho$  and that the energy of a system can be expressed in terms of a universal functional:

$$E[\rho] = T[\rho] + V_{eN}[\rho] + V_{ee}[\rho] \quad (3.40)$$

The ground state density can be obtained by minimizing the energy  $E_0 = \min_\rho E[\rho]$ . The main challenge is that the operators  $\hat{V}_{ee}$  and  $\hat{T}$  are unknown. To make a good approximation of the operators one can either base it on theoretical consideration, empirical fitting or semi-empirical approach. One of the approaches made is via the Kohn-Sham equation, often referred to



as Kohn-Sham DFT [24]. The approach views the density  $\rho$  as a sum of disconnected one-particle functions  $\phi_i$ :

$$\rho(r) = 2 \sum_i^{N/2} |\phi_i(r)|^2 \quad (3.41)$$

The major assumption, which leads to an approximation, that the kinetic energy is known for the individual parts of the disconnected system. The expectation value of the kinetic energy operator becomes:

$$T_s[\rho] = \langle \phi_i | -\frac{1}{2} \nabla^2 | \phi_i \rangle \quad (3.42)$$

which is not the true kinetic energy, a small part is missing. Similarly we can extract the classically defined self interaction of the density:

$$J[\rho] = \frac{1}{2} \int \int \frac{\rho(r)\rho(r')}{||r-r'||} dr dr' = \frac{1}{2} \int \rho(r) v_{el}(r) dr \quad (3.43)$$

which again is missing a small part of the true energy.

This means that the energy calculated in equation 3.40 can be rewritten as:

$$E[\rho] = T_s[\rho] + V_{eN}[\rho] + J[\rho] + E_{xc}[\rho] \quad (3.44)$$

where  $E_{xc}[\rho]$ , called exchange-correlation energy, represents the missing parts of  $J$  and  $T$

$$E_{xc}[\rho] = T[\rho] - T_s[\rho] + V_{ee}[\rho] - J[\rho] \quad (3.45)$$

Minimizing the energy by differentiation of equation 3.44 with respect to  $\rho$  gives:

$$\mu = \frac{\delta T_s[\rho]}{\delta \rho(r)} + v_{eff} \quad (3.46)$$

where the chemical potential  $\mu$  is a Lagrange multiplier and  $v_{eff}$  is as described in equation 3.47.

$$v_{eff} = \frac{\delta V_{eN}}{\delta \rho(r)} + \frac{\delta V_{el}}{\delta \rho(r)} + \frac{\delta E_{xc}}{\delta \rho(r)} \quad (3.47)$$

The Euler equation (3.46) describes a system of non-interacting electrons in an effective potential  $v_{eff}$ . The Hamiltonian for this kind of system is given by:

$$\hat{H} = - \sum_i^{N/2} \frac{1}{2} \nabla_i^2 + \sum_i^{N/2} v_{eff}(r_i) \quad (3.48)$$

Because this operator operates on a set of disconnected densities, the operator is separable and we obtain the Kohn-Sham equation:

$$\left(-\frac{1}{2}\nabla^2 + v_{eN}(r) + v_{el}(r) + v_{xc}(r)\right)\phi_i(r) = \epsilon\phi_i(r) \quad (3.49)$$

This means that the orbitals are back, and the hope of expressing the problem in terms of a single three-dimensional function  $\rho$  is gone. Because the potential  $v_{eff}$  in the Kohn-Sham equation is determined by the density, the solution method is the same as the HF equation (3.38).

$$\phi_i^{n+1}(r) = -2\hat{\mathcal{H}}^\nu[v_{eff}^n\phi_i^n](r) \quad (3.50)$$

### 3.4 Energy calculation with multi-wavelets

After the orbitals  $\phi_i$  have converged in the HF approaches or the DFT approach and their respective orbital energies  $\epsilon_i$  are known, the total energy of a system can be computed. In addition to the orbital energies we have the constant nuclear-nuclear repulsion  $\hat{V}_{NN}$  (3.6). The method of calculating the energy in HF and DFT for a MW basis both have the same goal, to avoid applying the kinetic energy operator  $\hat{T}_e$  (3.3).

#### 3.4.1 Energy calculations for Hartree-Fock

In this section, calculating the energy of a closed-shell molecule with an even number of electrons (doubly occupied orbitals) are discussed. The inclusion of solvent effect in the energy calculations is discussed in chapter 4.

First, the expectation value for a closed shell system:

$$E = \sum_{i=1}^{N/2} \langle \phi_i | \hat{h}_i | \phi_i \rangle + \frac{1}{2} \sum_{i=1}^{N/2} 2 \langle \phi_i | 2\hat{J}_j - \hat{K}_j | \phi_i \rangle \quad (3.51)$$

$$E = \sum_{i=1}^{N/2} 2 \langle \phi_i | \hat{T}_e | \phi_i \rangle + \sum_{i=1}^{N/2} 2 \langle \phi_i | v_{eN} | \phi_i \rangle + \sum_{i=1}^{N/2} \langle \phi_i | v_{el} - \hat{K} | \phi_i \rangle$$

$$E = \sum_{i=1}^{N/2} \langle \phi_i | 2\hat{T}_e - \hat{K} | \phi_i \rangle + \int \rho(r)v_{eN}dr + \frac{1}{2} \int \rho(r)v_{el}dr \quad (3.52)$$

where it is important to note that in the second part of 3.51. The 1/2 factor is to correct for the double counting done in  $\hat{J}$  and  $\hat{K}$ , the first 2 is for closed shell (double occupation for each  $i$ ), the second 2 is to correct for the spin.

The second 2 factor is missing for  $\hat{K}$ , this is due to the orthogonality of the spin. The kinetic energy operator ( $\hat{T}_e$ ) is avoided by noting that

$$\begin{aligned} \sum_i^{N/2} 2\epsilon_i &= \sum_i^{N/2} 2 \langle \phi_i | \hat{T}_e + v_{eN} + v_{el} - \hat{K} | \phi_i \rangle \\ \sum_i^{N/2} 2\epsilon_i &= \sum_i^{N/2} 2 \langle \phi_i | \hat{T}_e - \hat{K} | \phi_i \rangle + \int \rho(r) v_{eN} dr + \int \rho(r) v_{el} dr \end{aligned} \quad (3.53)$$

which by subtracting from 3.51 gives:

$$E = 2 \sum_i^{N/2} \epsilon_i - \sum_i^{N/2} \langle \phi_i | \hat{K} | \phi_i \rangle - \frac{1}{2} \int \rho(r) v_{el}(r) dr \quad (3.54)$$

Equation 3.54 is a way to express the energy without the kinetic energy operator, which is feasible for a MW basis, even though the Poisson operator ( $\hat{\mathcal{P}}$  in  $\hat{K}$ ) is applied.

### 3.4.2 Energy calculations for Density Functional Theory

In the deduction of the energy we assume a closed shell system with doubly occupied orbitals. The inclusion of solvent effect for the energy calculations with DFT is discussed in chapter 4. The energy functional for a Kohn-Sham DFT calculation was given in equation 3.44.

$$E[\rho] = T_s[\rho] + V_{eN}[\rho] + J[\rho] + E_{xc}[\rho] \quad (3.55)$$

which gives:

$$E = \sum_i^{N/2} 2 \langle \phi_i | \hat{T}_e | \phi_i \rangle + \int \rho(r) v_{eN} dr + \frac{1}{2} \int v_{el} \rho(r) dr + \int F_{xc} dr \quad (3.56)$$

The sum of the orbital energy contributions can similarly to the HF be expressed as:

$$\sum_i^{N/2} 2\epsilon_i = \sum_i^{N/2} 2 \langle \phi_i | \hat{T}_e | \phi_i \rangle + \int \rho(r) (v_{eN}(r) + v_{el}(r) + v_{xc}) dr \quad (3.57)$$

Subtracting the sum over the orbital energy from the total energy gives:

$$E = 2 \sum_i^{N/2} \epsilon_i - \frac{1}{2} \int \rho(r) v_{el} dr + \int F_{xc} dr - \int \rho(r) v_{xc} dr \quad (3.58)$$

which again is an energy expression without the use of  $\hat{T}_e$ . It is important to note that  $\int \rho(r)v_{xc} \neq \int F_{xc}dr$ .  $v_{xc} = \partial E_{xc}/\partial \rho(r)$  and  $\int F_{xc} = E_{xc}[\rho]$ . The functional  $F_{xc}$  is the specific approximated exchange correlation operator that varies with each DFT method.

# Chapter 4

## Solvation Models

### Contents

---

<b>4.1 Solvation Models . . . . .</b>	<b>37</b>
4.1.1 The all inclusive discrete method . . . . .	38
4.1.2 Continuum models . . . . .	39
<b>4.2 PCM for GTO . . . . .</b>	<b>40</b>
4.2.1 Cavity formulation using Tesserars . . . . .	41
<b>4.3 PCM for MW . . . . .</b>	<b>43</b>
4.3.1 Solvent effect potential inclusion in HF . . . . .	44
4.3.2 Solvent effect potential inclusion in DFT . . . . .	44
<b>4.4 Solvent energy with MW . . . . .</b>	<b>44</b>
4.4.1 Solvent energy calculations for wavelet Hartree-Fock	45
4.4.2 Solvent energy calculations for wavelet Density Func-	
tional Theory . . . . .	45

---

In a lab setting we never find a single molecule in vacuum. This is why precise calculations on molecules in a realistic environment are important. This is why many computational chemists work to improve their codes to include solvent effect. In this chapter we will look closer on how a molecule reacts to liquid solvents.

### 4.1 Solvation Models

This part of the thesis will focus on the representation and calculation of the effects of solvent on molecular systems. The effects of solvation can be viewed

as a sort of perturbation which is added to the gas phase Hamiltonian.

$$\hat{H}_{tot} = \hat{H}_g + \hat{H}_r \quad (4.1)$$

where  $\hat{H}_r$  is the operator that approximates how much the energy changes in relation to the environment,  $\hat{H}_g$  is the gas phase Hamiltonian discussed in chapter 3.

Solvent models are often divided into two categories; discrete models and a continuum models. A brief introduction to the discrete model is included as well as a more in depth discussion of the continuum models.

### 4.1.1 The all inclusive discrete method

The discrete method explicitly includes the solvent molecules in the Quantum Mechanics (QM) calculations. This means that all the effects of the solvent are calculated at the same level as the solute. This method is easily advocated in the physics of a solvent/solute system, the solvent is after all built up of discrete molecules. The method has its drawbacks. To reach a reasonable accuracy one needs to include a vast number of solvent molecules, which is not feasible for more than very small systems. Even then the source of error due to the number of solvent molecules included and their orientation will be vast.

To use this method in a reasonable time scale, a number of approximations have been postulated. Molecular Mechanics (MM) methods is one of them. MM methods view the solvent from a classical point of view with a chemical force field and the solute from a QM view. In the MM region, one atom is considered as one particle, typically with a van der Waals (vdW) radius, charge and polarizability. The most popular QM/MM method is the electrostatic embedding, where the solvent part of the Hamiltonian in operator 4.1

$$\hat{H}_r = \hat{H}_{QM/MM} + \hat{H}_{MM} \quad (4.2)$$

is split in two.  $\hat{H}_{QM/MM}$  contains the electrostatic interaction between the QM and MM subsystems.  $\hat{H}_{MM}$  is a completely classical term which represents the interactions within the MM part of the system. The  $\hat{H}_{QM/MM}$  operator generally corresponds to a one-electron operator, which is combined with the electrostatic operator for the electron-nuclear operator from the QM region:

$$\hat{H}_{QM/MM}^{el} = \sum_m q_m \hat{V}(r_m) \quad (4.3)$$

where  $\hat{V}(r_m)$  is the electrostatic potential due to the QM system calculated at the MM site  $m$ .  $q_m$  is the partial atomic charges representing the MM sites. The issue with this kind of approach is that the operator  $\hat{H}_{QM/MM}$  allows the QM part to be polarized by the surrounding MM subsystem, but not the other way around. To render this issue, it is possible to account for the mutual polarizable effect by using polarizable embedding. Examples of this are the fluctuating charges [25], Drude oscillators [26] or the induced-dipoles [27].

The QM/MM method is not only applicable for liquid solvents. The method is widely used for computations on big molecules where only a part of the molecule is of interest. This is often the case for medical computational chemistry where protein structures are a big factor.

Applying MM makes the calculations faster, but one still has to consider a large number of solvent conformations. With these methods one often has to rely on chemical intuition, especially for the conformations of the solvent molecules.

### 4.1.2 Continuum models

The second category of solvation model is the continuum model. Unlike the discrete approach the solute/solvent energy is perturbed by the electrostatic interaction from a dielectric continuum solvent. These models describe the solvent with dielectric continuum, meaning that the solvent is represented by a statistical average of the solvent molecules' conformation and properties. The statistical average is typically represented by macroscopic properties such as dielectric constant, density etc. Comparing the two methods gives us a preliminary outline for further discussion:

- The continuum model decreases the computational efforts that are needed for the calculation, meaning shorter computational time.
- The function representing the solvent can easily be manipulated to contain any sort of macroscopic property.
- The user usually needs less chemical intuition to run calculations. The main reason for this is that the conformation of the solvent molecules is not of concern to the user.
- The accuracy of calculation might be reduced, precisely because of the solvent conformations. Continuum models sometimes have problems with important intermolecular bonding between solvent and solute. Multiscale modelling appears to be a viable resolution to this problem [28].

The continuum models presented in this thesis are based on the Poisson equation, derived from Maxwell's equations:

$$\nabla \vec{D} = 4\pi\rho \quad (4.4)$$

$$\vec{D} = -eps\nabla V \quad (4.5)$$

which results in the Poisson equation:

$$-\nabla \cdot (\varepsilon(\vec{r})\nabla V(\vec{r})) = 4\pi\rho(\vec{r}) \quad (4.6)$$

where  $\rho$  is the total charge density,  $\varepsilon(\vec{r})$  is the position dependent permittivity function and  $V(r)$  is the electrostatic potential.

The two models presented are the Apparent Surface Charge (ASC) model with Gaussian-Type Orbital (GTO) and Surface and Volume Polarization of Electrostatics (SVPE) model with MultiWavelet (MW). Both methods can be considered a form of Polarizable Continuum model (PCM), where the solvent affects the electrostatic potential of the solute via polarization.

## 4.2 Polarizable Continuum Model for Gaussian-type basis-sets

Starting from the Poisson equation (4.6), we need to represent the dielectric function  $\varepsilon(r)$ . Under the assumption that the total charge density  $\rho$  is contained within the cavity,  $\varepsilon(r)$  is split in two:

$$\varepsilon(r) = \begin{cases} 1 & , \vec{r} \in C \\ \varepsilon_\infty & , \vec{r} \notin C \end{cases} \quad (4.7)$$

This means that the Poisson equation (4.6) can be split in two, one inside the cavity and one outside:

$$\begin{aligned} -\nabla^2 V(\vec{r}) &= 4\pi\rho(\vec{r}) & ; \vec{r} \in C \\ -\varepsilon_\infty \nabla^2 V(\vec{r}) &= 0 & ; \vec{r} \notin C \end{aligned} \quad (4.8)$$

with the following boundary conditions:

$$\begin{aligned} V_{in}(\vec{s}) &= V_{out}(\vec{s}), \quad \vec{s} \in \partial C \\ \left. \frac{\partial V}{\partial \vec{n}} \right|_{in} &= \varepsilon_\infty \left. \frac{\partial V}{\partial \vec{n}} \right|_{out} \end{aligned} \quad (4.9)$$

where  $\vec{s}$  represents a point on the surface of the cavity. At this point, we can assume that the vacuum potential  $V_{vac}$  is known. To solve the electrostatic



equation (4.8) we write the potential  $V$  as a sum of the potential arising from the charge density inside  $C$  labeled  $V_{vac}$  plus the potential contribution from polarization of the dielectric labeled  $V_r$ .

$$V(\vec{r}) = V_{vac}(\vec{r}) + V_r(\vec{r}) \quad (4.10)$$

The potential inside the cavity ( $V_{vac}$ ) is the same as the solutions of the Schrödinger Equation (SE) of the gas phase calculations in chapter 3.  $V_r$ , commonly known as the reaction potential, is in integral representation:

$$V_r(\vec{r}) = \int_{\partial C} \frac{\sigma(\vec{s})}{|\vec{r} - \vec{s}|} \quad (4.11)$$

where the apparent surface charge  $\sigma$  is the fictional charge introduced on the boundary between the solvent and the solute. The surface charge  $\sigma$  is the solution of an integral equation on  $\partial C$

$$(A\sigma)(\vec{s}) = \hat{\mathcal{P}}[\sigma(\vec{s}')](\vec{s}) = b_\rho(\vec{s}) \quad (4.12)$$

where the integral operator  $A$  and  $b_\rho$  varies from method to method, the common denominator is that  $b_\rho$  is linearly dependent on  $\rho$ . A way to simplify this equation is to introduce point charges on  $\partial C$ .

### 4.2.1 Cavity formulation using Tesserars

The goal of this section is to describe how and why the representation via tesserars is used. Starting from a one atom system, meaning that  $C$  is a spherical symmetric ball, one needs to restrict the solvent from being in an unphysical distance from the solute atom. This means that the radius of  $C$  usually is written as the vdW radius or some scalar multiple of that. The simplest way to represent a sphere in space is by use of spherical coordinates, but it is apparent that this representation will not hold. The reason for this is that the data points will not be evenly spaced, the spherical coordinates representations lead to a cluster of data points around the poles of the cavity and too few points around equator (exactly like longitude and latitude lines on a globus). The cavity  $C$  needs to be represented numerically and by evenly (or close to evenly) spaced points. There are two reasons for this. Firstly, the evenly spaced points on the spherical cavity make it easier to obtain a surface that is as smooth as possible while using the fewest number of points. Secondly, the continuous ASC  $\sigma$  needs to be discretized into point charges and with the points evenly spaced, the weight  $a_i$  of each point charge  $q_i$  is of the same size (or close to the same size).

$$\sigma(\vec{s}) = \sum_i a_i q_i \quad (4.13)$$

This reduces the computational efforts compared to the spherical coordinates representation. The most common way of making a sphere is (in short) by starting from a polyhedron built up of polygons, then increase the number of polygons until the preferred accuracy is obtained. This method of making a sphere is often referred to as tessellation or Hierarchical Triangular Mesh (HTM)[29]. Although some structures are better than others, any kind of polyhedron and polygons may be used. In the following deduction we will use an octahedron built from triangles as these are shapes most chemist are comfortable with.

If we start from an octahedron we have 7 data points (six corners and a center) and 8 sides (fig: 4.1). Viewing one of these triangles, made up of 3 points and 3 lines, we can find 3 new points, 1 for each line, that are exactly midway between 2 points. Drawing new lines between the 3 new points gives us a

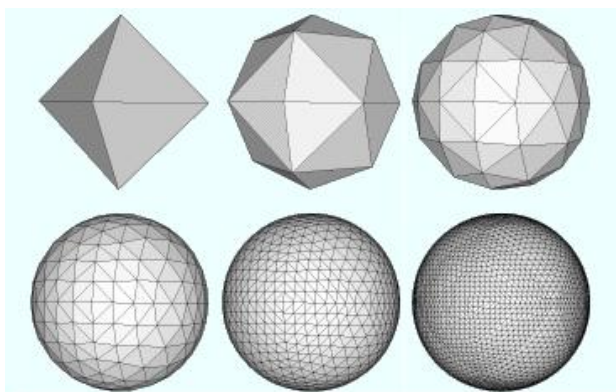


Figure 4.1: [30]

subdivision of the original triangle into 4 smaller triangles. The 3 new points are then scaled to the surface ( $\partial C$ ) of the sphere ( $C$ ) by a simple scalar multiplication by the predetermined radius of the sphere. This is done for every side of the octahedron, which makes a new polyhedron with  $(8 * \frac{3}{2} + 6 + 1)$  19 data points producing  $(8 * 4)$  32 triangles. These triangles produce 3 new points but each point is produced twice plus the original 7 and each original triangle produces 4 new triangles. Applying the procedure iteratively, we obtain a convergence of the volume of the sphere  $V_C = \frac{4}{3}\pi r_C^3$ .

With the tessalated cavity in place, it is possible to represent the total ASC function  $\sigma$ . Each tessera (triangle), on  $\partial C$ , is associated with an ASC point charge  $q_i$ . The area of the tessera can be used directly as the weight  $a_i$  in equation 4.13, which allows us to calculate the electrostatic reaction potential (4.11).

With the formulation of the tesserae we can rewrite equation 4.11:

$$V_r(\vec{r}) = \frac{\sum_i a_i q_i}{|\vec{r} - \vec{s}|} \quad (4.14)$$

which means that we can rewrite the integral equation (4.15) to its analog matrix equation:

$$(A\sigma)(\vec{s}) = \hat{\mathcal{P}}[\sigma(\vec{s}')](\vec{s}) \quad (4.15)$$

$$\mathbf{Q}\vec{q} = -\mathbf{R}f_M^{\vec{}} \quad (4.16)$$

where vector  $\vec{q}$  and  $f_M^{\vec{}}$  are vectors containing the values of the charge and of the solute electrostatic potential at each point on the surface mesh.  $\mathbf{Q}$  and  $\mathbf{R}$  are the matrix analogs of the integral operators,  $A$  and  $\hat{\mathcal{P}}$ .

### 4.3 Polarizable Continuum Model for multi-wavelet basis

Solving the Poisson equation in MW can be done with the SVPE method. The equation is the same as for the GTO-PCM case (4.6). The derivations in this section follows that of Harrison [31].

The difference between the two equations is that  $\varepsilon(r)$  is discontinuous for the ASC case, making it possible to split the equation in two. In the MWs basis,  $\varepsilon(r)$  is defined as a continuous function with a smooth transition from solvent to solute, the specifics of how it is made and implemented are discussed in chapter 5. The splitting of the Poisson equation is not possible for a continuous function, but by rewriting the Poisson equation we can reuse the Poisson operator ( $\hat{\mathcal{P}}$ ) used in the Hartree-Fock (HF) and Density Functional Theory (DFT) Self-Consistent Field (SCF):

$$\begin{aligned} -\nabla \cdot (\varepsilon(r)\nabla V(r)) &= 4\pi\rho(r) \\ \nabla\varepsilon(r)\nabla V(r) + \varepsilon(r)\nabla^2 V(r) &= 4\pi\rho(r) \\ \nabla^2 V(r) &= -\frac{4\pi\rho(r)}{\varepsilon(r)} - \frac{\nabla\varepsilon(r)\nabla V(r)}{\varepsilon(r)} \\ \nabla^2 V(r) &= -\rho_{eff} - \gamma_s \end{aligned} \quad (4.17)$$

where the first part ( $\rho_{eff}$ ) is the effective volume charge distribution and  $\gamma_s$  is the surface charge distribution. Once again, by applying the Poisson operator  $\hat{\mathcal{P}}$  the solution algorithm is an iterative process:

$$V^{m+1}(r) = \hat{\mathcal{P}}[\rho_{eff}^n + \gamma^m](r) \quad (4.18)$$

### 4.3.1 Solvent effect potential inclusion in HF

To include the solvent effect ( $\hat{V}_r$ ) in the HF for the wavelet-basis is a matter of including an additional scalar multiplication operator  $v_r$  in equation 3.37:

$$v_{eff} = v_{eN} + v_{el} + v_r \quad (4.19)$$

which combines all three operators into one, the  $v_{eff}$ . The new HF equation then becomes:

$$\left( -\nabla^2 - 2\epsilon_i \right) \phi_i = -2 \left( v_{eff} - \hat{K} \right) \phi_i \quad (4.20)$$

The reaction potential ( $\hat{V}_r$ ) approximation is not straightforward. The main problem is that that  $\hat{V}_r$  is a function of  $\phi_i$  (or rather  $\rho$ ). A detailed discussion is found in chapter 5.

Assuming that  $v_{eff}$  is known, equation 4.20 can be solved with the SCF procedure (3.38):

$$\phi_i^{n+1}(r) = -2\hat{\mathcal{H}}^\nu [(v_{eff} - \hat{K}^n)\phi_i^n](r) \quad (4.21)$$

### 4.3.2 Solvent effect potential inclusion in DFT

The inclusion of solvent effect in DFT is a matter of adding the effects of the solvent-solute interaction in the universal energy functional (3.44):

$$E[\rho] = T_\sim[\rho] + V_{eN}[\rho] + J[\rho] + E_{xc}[\rho] + E_r[\rho] \quad (4.22)$$

where

$$E_r[\rho] = \frac{1}{2} \int \rho(r) v_r dr \quad (4.23)$$

for a closed shell system. In the solvent DFT case,  $v_r$  is included in  $v_{eff}$ ;

$$v_{eff} = \frac{\delta V_{eN}}{\delta \rho(r)} + \frac{\delta V_{el}}{\delta \rho(r)} + \frac{\delta E_{xc}}{\delta \rho(r)} + \frac{\delta E_r}{\delta \rho(r)} \quad (4.24)$$

which, by assuming that  $v_r$  is known, gives the same solution algorithm as 3.50

## 4.4 Solvent energy calculation with multi-wavelets

This section includes the solvent effect potential energy ( $v_r$ ) in the energy calculations performed in HF and DFT. The deductions performed will be less comprehensive than for the solvent free case, see chapter 3 for a more detailed presentation.

#### 4.4.1 Solvent energy calculations for wavelet Hartree-Fock

The inclusion of  $v_r$  in the calculation of the energy will again be formulated without the use of the kinetic operator  $\hat{T}_e$ . The solvent energy expectation value for a closed shell system is:

$$\begin{aligned}
 E &= \sum_{i=1}^{N/2} \langle \phi_i | \hat{h}_i | \phi_i \rangle + \frac{1}{2} \sum_{i=1}^{N/2} 2 \langle \phi_i | 2\hat{J}_j - \hat{K}_j | \phi_i \rangle + \sum_i^{N/2} \langle \phi_i | v_r | \phi_i \rangle \\
 E &= \sum_{i=1}^{N/2} \langle \phi_i | 2\hat{T}_e - \hat{K} | \phi_i \rangle + \int \rho(r) v_{eN} dr + \frac{1}{2} \int \rho(r) v_{el} dr + \frac{1}{2} \int \rho(r) v_r dr
 \end{aligned} \tag{4.25}$$

The kinetic energy operator ( $\hat{T}_e$ ) is again avoided by use of the orbital energies  $\epsilon_i$ :

$$\sum_i^{N/2} 2\epsilon_i = \sum_i^{N/2} 2 \langle \phi_i | \hat{T}_e - \hat{K} | \phi_i \rangle + \int \rho(r) v_{eN} dr + \int \rho(r) v_{eN} dr + \int \rho(r) v_r dr \tag{4.26}$$

which by subtracting from 4.25 gives:

$$E = 2 \sum_i^{N/2} \epsilon_i - \sum_i^{N/2} \langle \phi_i | \hat{K} | \phi_i \rangle - \frac{1}{2} \int \rho(r) v_{el}(r) dr - \frac{1}{2} \int \rho(r) v_r(r) dr \tag{4.27}$$

#### 4.4.2 Solvent energy calculations for wavelet Density Functional Theory

The solvent energy functional for a Kohn-Sham DFT calculation was given in equation 4.22.

$$E[\rho] = T_{\sim}[\rho] + V_{eN}[\rho] + J[\rho] + E_{xc}[\rho] + V_r[\rho] \tag{4.28}$$

which gives:

$$E = \sum_i^{N/2} 2 \langle \phi_i | \hat{T}_e | \phi_i \rangle + \int \rho(r) v_{eN} dr + \frac{1}{2} \int v_{el} \rho(r) dr + \frac{1}{2} \int v_r \rho(r) dr + \int F_{xc} dr \tag{4.29}$$

The sum of the orbital energy contributions can similarly to the HF be expressed as:

$$\sum_i^{N/2} 2\epsilon_i = \sum_i^{N/2} 2 \langle \phi_i | \hat{T}_e | \phi_i \rangle + \int \rho(r) (v_{eN}(r) + v_{el}(r) + v_r(r)) dr \quad (4.30)$$

Subtracting the sum of the orbital energy from the total energy gives:

$$E = 2 \sum_i^{N/2} \epsilon_i - \frac{1}{2} \int \rho(r) v_{el} dr - \frac{1}{2} \int \rho(r) v_r(r) dr + \int F_{xc} dr - \int \rho(r) v_{xc} dr \quad (4.31)$$

which again is an energy expression without the use of  $\hat{T}_e$ .

# Chapter 5

## Implementation

### Contents

---

<b>5.1 Cavity implementation</b>	<b>47</b>
5.1.1 The interlocking sphere approach and representation of $\varepsilon(r)$	48
<b>5.2 SCF implementation</b>	<b>49</b>
5.2.1 Pilot code	50
5.2.2 Full implementation	53

---

This section contains the specifics of how the theories from earlier chapters were implemented in MRChem. Keep in mind that for the descriptions of the code in this chapter, the gory details of projecting functions and operators onto the MultiWavelet (MW) basis are not included. Note also that the implementations are closely connected to the equations presented. This is an effect that emerges when the basis gives the possibility of working directly with the orbitals and densities vs. working on their representation in a Gaussian-Type Orbital (GTO) basis.

### 5.1 Cavity implementation

In a wavelet basis the procedure of tessellation does not hold for the representation of the cavity. This means that a new approach to the cavity implementation had to be adopted to perform solvent effect energy calculations in MRChem [1]. The way this was done was via the interlocking sphere method described in [31]. Because of the different representation of the cavity, there is a different representation of the dielectric function  $\varepsilon(r)$ .

$\varepsilon(r)$  is represented as a smooth function instead of the discontinuous  $\varepsilon(r)$  used for GTO (4.7). This results in a different solution algorithm as well.

### 5.1.1 The interlocking sphere approach and representation of $\varepsilon(r)$

The implementation of the cavity starts by defining a sphere around each nucleus:

$$s_I = |r - r_I| - R_I \quad (5.1)$$

where  $r_I$  is the nuclear center,  $R_I$  is the van der Waals (vdW) radius of atom  $I$ . Next, we introduce the characteristic sphere around atom  $I$ :

$$C_I(r) = 1 - \Theta(s_I(r)) \quad (5.2)$$

where, for now,  $\Theta$  is the Heaviside stepping function that is defined as 1 outside, 0 inside and 1/2 on the cavity:

$$\Theta(s) = \begin{cases} 0 & \text{for } s < 0 \\ \frac{1}{2} & \text{for } s = 0 \\ 1 & \text{for } s > 0 \end{cases} \quad (5.3)$$

$C_I$  is then a function that is 1 inside, 0 outside and 1/2 on the cavity:

$$C_I(\Theta) = \begin{cases} 1 & \text{for } \Theta = 0 \\ \frac{1}{2} & \text{for } \Theta = 1/2 \\ 0 & \text{for } \Theta = 1 \end{cases} \quad (5.4)$$

Taking the product of the spheres around each atom leads to the total cavity of any system:

$$C(r) = 1 - \prod_{I=1}^N (1 - C_I(r)) \quad (5.5)$$

Again, defined as 1 inside, 0 outside and 1/2 on the cavity.

Replacing the Heaviside function with a smooth function, we obtain a smooth transition from solvent to solute:

$$\Theta(s_I/\sigma) = \frac{1}{2}(1 + \operatorname{erf}(s_I/\sigma)) \quad (5.6)$$



where  $\sigma$  is the width of the smooth transition, referred to as "slope".

With the cavity represented, we can use it to represent the dielectric function  $\varepsilon(r)$ :

$$\varepsilon(r) = \varepsilon_0 e^{\ln(\frac{\varepsilon_\infty}{\varepsilon_0})(1-C(r))} \quad (5.7)$$

and the multiplicative inverse of  $\varepsilon(r)$

$$\varepsilon(r)^{-1} = \varepsilon_0^{-1} e^{\ln(\frac{\varepsilon_0}{\varepsilon_\infty})(1-C(r))} \quad (5.8)$$

Note that while  $\Theta$  is symmetric around the vdW radius,  $\varepsilon(r)$  is not.

A simplified pseudocode is written in 5.1 where the analytic functions  $\varepsilon(r)$  and  $\varepsilon(r)^{-1}$  are returned. The functions then have to be projected onto the MW basis.

Listing 5.1: Evaluating dielectric function  $\varepsilon(r)$

```

\varepsilon(r) {
  for (I in nuclei) {
    s_I = |r - r_I| - R_I
    \Theta_I = 1/2 * (1.0+erf(s_I/\sigma))
    C_I = 1.0 - \Theta_I
  }

  C_tot = 1.0;
  for (I in nuclei) {
    C_tot *= 1.0 - C_I
  }
  C_tot = 1.0 - C_tot

  //Return function \varepsilon or \varepsilon^{-1}
  if (inverse) {
    return 1.0/\varepsilon_0 * exp(log(\varepsilon_0/\varepsilon_\infty)(1.0 - C_tot))
  } else {
    return \varepsilon_0 * exp(log(\varepsilon_\infty/\varepsilon_0)(1.0 - C_tot))
  }
}

```

With a smooth  $\varepsilon(r)$  and  $\varepsilon(r)^{-1}$  implemented, the Self-Consistent Field (SCF) algorithm can be discussed.

## 5.2 SCF implementation

The implementation of the solvent effect in MRChem was done in three stages.

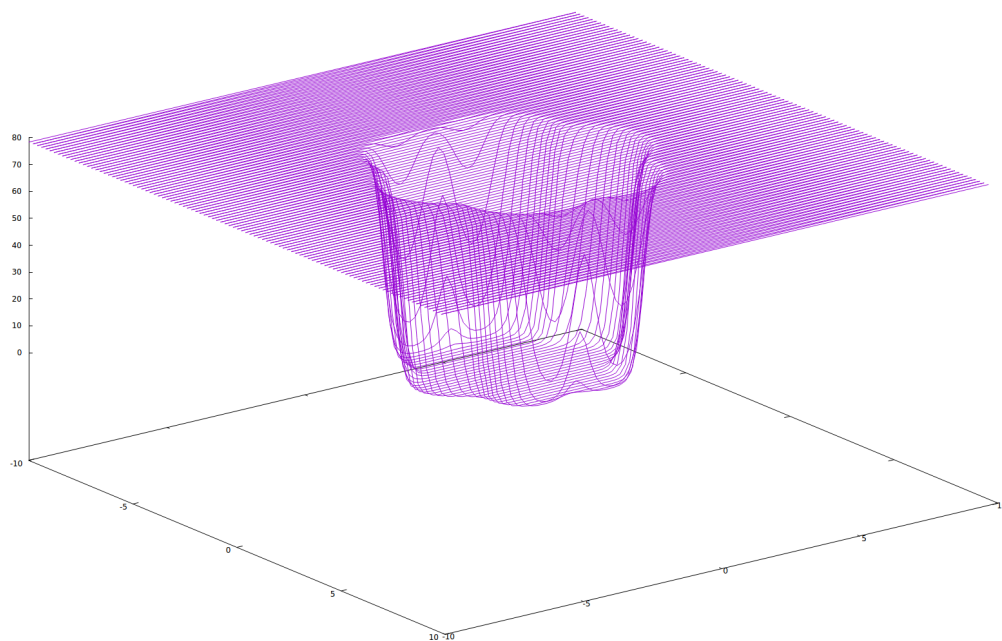


Figure 5.1:  $\epsilon(r)$  for benzene ( $C_6H_6$ ) with slope  $\sigma = 0.4$ ,  $\epsilon_\infty = 78.304$  plotted with Gnuplot[32]

1. A pilot implementation of the iterative process for solving the Poisson equation (4.18). This will, in addition to the Hartree-Fock (HF) and Density Functional Theory (DFT) SCF, be referred to as a SCF.
2. The pilot implementation was expanded to include the solvent effect HF-SCF for mono-atomic systems with at most 2 electrons. Testing was performed for different slopes and compared with PCMSOLVER [33]
3. Full implementation. The solvent effects were combined with the already existing framework for solvent free HF and DFT. The code was tested against Gaussian for a variety of molecules, precisions and slopes.

The description of the different parts is discussed in two sections, first the pilot code and then the full implementation.

### 5.2.1 Pilot code

The pilot code was designed to calculate the orbitals  $\phi$ , the reaction potential  $v_r$  as well as the total potential  $V$ . The solutions to the Poisson equation is the total  $V$ , while  $V_r$  is a "bi-product". The iterative process that was

implemented is described in equation 4.18. The main structure of the code is written in listing 5.2, the pseudo-code illustrates the procedure developed to manage two different SCFs. The two different SCFs will be referred to as potential-SCF ( $V$ -SCF) or orbital-SCF ( $\phi$ -SCF). It is important at this stage to underline the fact that the  $V$ -SCF is an algorithm determined by the total density ( $\rho = \rho_{el} + \rho_{nuc}$ ) and that the  $\phi$ -SCF is determined by  $\rho_{el}(\phi)$ .

Listing 5.2: The double SCF procedure

```

SCF( prec , nucs , rho_nuc , rho_el , eps_0 , eps_inf , invers ) {

     $\varepsilon$ ( nucs , slope ,  $\varepsilon_0$  ,  $\varepsilon_\infty$  , inverse ) [5.1]
    make{ rho_nuc , V_nuc };
     $\rho = \rho_{el}^n + \rho_{nuc}$ ;

    error_phi = 10.0*prec;
    while ( error_phi > prec ) {
        if ( error_phi < 10.0*prec ) {
            while ( error_V > prec ) {
                calcV(  $V_m$  ,  $\rho$  ,  $\varepsilon$  ,  $\varepsilon_{inv}$  ,  $\nabla\varepsilon$  ); [5.4]
            }
        }
        calc $\phi$ (  $\phi_n$  ,  $V_{nuc}$  ,  $V_r$  ); [5.3]
    }
    energy(  $\phi^n$  ,  $V_r$  ,  $V_m$  );
}

```

Listing 5.2 shows that the two different while loops run over two different functions, the  $calcV$  and  $calc\phi$ . Prec is used as a parameter to determine how accurate the user wants the calculations to be, how  $calcV$  and  $calc\phi$  are implemented is described in listings 5.3 and 5.4. The double SCF *almost* converges the orbitals with  $v_r = 0$ , before the algorithm includes the solvent effect. This is forced with the if test. The if test also prevents the code from jumping between calculating  $V$  and  $\phi$  one to one.

Listing 5.3: orbital SCF

```

calc $\phi$ ( phi_n , V_nuc , V_r ) {
     $\rho_{el} = phi^n * phi^n$ ;
     $V_{el} = \text{po}(\rho_{el})$ ;
     $V\phi^n = (V_r + V_{nuc} + 0.5 * V_{el})\phi^n$ ;

    calcEnergy ();
     $\nu_n = \text{sqrt}(-2E_n)$ ;
     $\phi^{n+1} = \hat{\mathcal{H}}^\nu(V\phi^n)/2\pi$ ;
}

```

```

 $\Delta\phi^n = \phi^{n+1} - \phi^n$ 
if ( $\|\Delta\phi_i^n\| < \text{error\_phi}$ ) return;

error_V      = 1.0;
}
}

```

Listing 5.3 shows the basic  $\phi$ -SCF for a one-atom two-electron system, with the addition of  $\text{error\_V} = 1.0$ .  $\text{error\_V}$  needs to be updated, otherwise the algorithm would only visit the  $V$ -SCF once.

The  $V$ -SCF described in listing 5.4 describes how the approximations of the reaction potential  $v_r$  were performed.  $v_r$  is defined as the potential difference between that gas-phase calculations and the total potential:

$$v_r = \hat{\mathcal{P}}[\gamma + \rho_{eff} - \rho](r) \quad (5.9)$$

or equivalently:

$$v_r = \hat{\mathcal{P}}\left[\gamma + \frac{(1 - \varepsilon(r))\rho}{\varepsilon(r)}\right](r) \quad (5.10)$$

where we assume that  $\gamma$  and  $\rho$  have converged and are known.

Listing 5.4: Pilot code for  $V$ -SCF approach

```

calcV ( $V^m, \rho, \varepsilon, \varepsilon_{inv}, \nabla\varepsilon$ ) {

  calc  $\nabla V$ ;
 $\gamma^m = \nabla\varepsilon * \nabla\hat{V}/\varepsilon$ ;
 $\rho_{eff} = \rho/(4\pi\varepsilon)$ ;
 $V^{m+1} = \hat{\mathcal{P}}(\rho_{eff} + \gamma)$ ;
 $\Delta V = V^{m+1} - V^m$ ;
if ( $\|\Delta V\| < \text{error\_V}$ ) return;

KAIN ( $V^m, \Delta V^m$ )  $\rightarrow$  ( $V^m, \delta V^m$ )

 $V^{m+1} = V^m + \delta V$ 

 $V_r = \hat{\mathcal{P}}(\gamma^m + \rho_{eff} - \rho)$ ;
}

```

The code returns (after convergence)  $V$  and computes  $v_r$  for further use in the  $\phi$ -SCF. It is important to note that  $v_r$  gives the possibility to calculate

how much the energy changes due to the solvent effect.

$$E_r = \langle \phi | v_r | \phi \rangle = \int \rho(r) v_r dr \quad (5.11)$$

To verify that the pilot code did what it was supposed to do, the following integrals were compared:

$$\int \gamma dr = \frac{1 - \varepsilon_\infty}{\varepsilon_\infty} \int \rho dr \quad (5.12)$$

which is a direct descendant of Gauss's Theorem. The integrals state that the integral over the surface charge distribution  $\gamma = \frac{\nabla \varepsilon(r) \cdot \nabla V(r)}{\varepsilon(r)}$  is equal to the integral over the total charge density  $\rho$  times  $\frac{1 - \varepsilon_\infty}{\varepsilon_\infty}$ .

### Krylov subspace accelerated inexact Newton Method

Due to numerical instabilities in the SCFs, a method of increasing the convergence rate has been implemented in MRCHEM . The method is called Krylov subspace Accelerated Inexact Newton Method (KAIN)[34]. Both in the  $\phi$ -SCFs and in the  $V$ -SCF, KAIN was used. The method is based on Newton's methods, and computes an approximation to the Jacobi matrix. The method gives an update of the function  $f$  ( $\phi$  or  $V$ ) which is better than the one used directly ( $f^{n+1} = f^n + \Delta f \rightarrow f^{n+1} = f^n + \delta f$ ). KAIN uses the information from the previous iterations to make a better guess for the next iteration.

## 5.2.2 Full implementation

The full implementation of the solvent effect in the HF method and DFT are closely related and will be described with one pseudocode.

Listing 5.5: Full implementation

```

calc  $\rho_{el} = \sum_i |\phi_i|^2$ 
calc  $V_{el}(\rho_{el}), V_{xc}(\rho_{el})$ 
calc  $V_r(\rho_{nuc}, \rho_{el})$ 
calc  $V\phi_i = (V_{nuc} + V_{el} + V_r + V_{xc} - \hat{K})\phi_i$ 

 $\phi_i^{n+1} = \hat{\mathcal{H}}^\nu[V\phi_i^n]$ 
 $\Delta\phi^n = \phi^{n+1} - \phi^n$ 
if ( $\|\Delta\phi_i^n\| < \text{error\_phi}$ ) return ;

KAIN ( $\psi^n, \Delta\phi^n$ )  $\rightarrow$  ( $\phi^n, \delta\phi^n$ )

```

```

|  $\phi^{n+1} = \phi^n + \delta\phi$ 
| // Normalize
|  $\langle \phi_i^{n+1} | \phi_j^{n+1} \rangle = \delta_{ij}$ 
|

```

The code (5.5) shows the procedure of one iteration of the solvent inclusion  $\phi$ -SCF. This means that the  $V$ -SCF is called as a simple function.

### Spillover effect

A bi-effect of the continuous dielectric function  $\varepsilon(r)$  used in the formalism of Polarizable Continuum model (PCM) in MW gives the possibility of calculating spillover effects.

$$\text{spillOver} = \int \frac{\varepsilon(r) - \varepsilon_0}{\varepsilon_\infty - \varepsilon_0} \rho dr \quad (5.13)$$

The spillover effect tells us how much of the charge density is located "outside" the cavity.

# Chapter 6

## Results

### Contents

---

<b>6.1</b>	<b>Pilot code</b>	<b>55</b>
<b>6.2</b>	<b>Full implementation</b>	<b>56</b>
6.2.1	Solvent energy	57
6.2.2	Solvent dipole Moment	59
<b>6.3</b>	<b>Concluding remarks and ideas for improvement</b>	<b>60</b>

---

Presenting results for this thesis presented a few problems. The combination of Surface and Volume Polarization of Electrostatics (SVPE) is a MultiWavelet (MW) method is relatively new. This means that there are few codes in the world that can do this, in fact, only one exist; MADNESS [11]. Obtaining useful results from MADNESS proved to be to difficult to do in the time frame of this thesis.

However, some tests and verifications can be done; The pilot implementation have been verified by Gauss' theorem 5.12. The full implementation was compared with GAUSSIAN[2]

The result section is divided in three main parts. The first contains calculations done with the pilot code. The second contains calculations done with the full implementation.

### 6.1 Pilot code

This section contains verifications that the  $V$ -Self-Consistent Field (SCF) is working as it should. The verification was done with Gauss' theorem (5.12). A spherical charge distribution  $\rho$  was set too  $\rho(r) = (\alpha/\pi)^{3/2}e^{-\alpha r^2}$ , so that  $\int \rho(r)dr = 1$ , with  $\alpha = 100$ . In the test cases, the reaction potential was

converged with precision  $10^{-3}$ ,  $10^{-4}$ ,  $10^{-5}$  and  $10^{-6}$  and the integral of the corresponding induced reaction charge  $\gamma$  was compared with the exact value ( $\frac{1-\epsilon_\infty}{\epsilon_\infty}$ ).

Table 6.1: Reaction charge generated from a spherical Gaussian distribution of unit charge with exponent  $\alpha = 100$ , centered in a spherical cavity of unit radius, and computed with two different slopes  $\sigma = 0.2, 0.4$ . Dielectric constant is that of benzene ( $\epsilon_\infty = 2.27$ ). Exact value computed from Gauss' theorem eq. (5.12).

Prec	Reaction charge	Error	Reaction charge	Error
	$\sigma = 0.2$		$\sigma = 0.4$	
$10^{-3}$	-0.554 985 726	4.4e-03	-0.559 317 865	1.5e-04
$10^{-4}$	-0.559 543 028	-7.1e-05	-0.559 322 308	1.4e-04
$10^{-5}$	-0.559 474 627	-3.2e-06	-0.559 464 890	6.4e-06
$10^{-6}$	-0.559 472 038	-6.7e-07	-0.559 472 053	-6.8e-07
Exact	-0.559 471 365		-0.559 471 365	

Table 6.2: Reaction charge generated from a spherical Gaussian distribution of unit charge with exponent  $\alpha = 100$ , centered in a spherical cavity of unit radius, and computed with two different slopes  $\sigma = 0.2, 0.4$ . Dielectric constant is that of water ( $\epsilon_\infty = 78.30$ ). Exact value computed from Gauss' theorem eq. (5.12).

Prec	Reaction charge	Error	Reaction charge	Error
	$\sigma = 0.2$		$\sigma = 0.4$	
$10^{-3}$	-0.983 925 412	3.3e-03	-0.986 280 718	9.4e-04
$10^{-4}$	-0.987 286 244	-5.7e-05	-0.987 244 101	-1.5e-05
$10^{-5}$	-0.987 230 349	-1.7e-06	-0.987 223 514	5.0e-06
$10^{-6}$	-0.987 228 034	5.7e-07	-0.987 228 402	2.0e-07
Exact	-0.987 228 607		-0.987 228 607	

The tests were done with benzene ( $\epsilon_\infty = 2.27$ ) and water ( $\epsilon_\infty = 78.30$ ) and with slopes  $\sigma = 0.2$  and  $0.4$ . The tests were proven successful.

## 6.2 Full implementation

The tables in this section compare the SVPE method used in MRChem with Apparent Surface Charge (ASC) calculations. It is important to note that these are different methods and thereby not directly comparable. SVPE for wavelets is a new approach, which makes the choices for verification and comparison limited. Nevertheless, GAUSSIAN, which is the program used for



ASC-Polarizable Continuum model (PCM), has been thoroughly tested. If the calculations done with MRChem are in the same ballpark, it is a strong indicator that the implementations of SVPE works. The quantities that have been calculated are energy and dipole moment for the Hartree-Fock (HF) method.

### 6.2.1 Solvent energy

There are four molecules that have been tested for the solvent energy calculations: One symmetric;  $H_2O$ , one non-symmetric  $CH_3CONH_2$ , one cation;  $NO^+$  and one anion;  $CN^-$ . Geometry optimization of  $H_2O$ ,  $NO^+$  and  $CH_3CONH_2$  were performed using GAUSSIAN with the basis set 6-31G\*\*,  $CN^-$  was optimized with 6-31+G\*\*[35].

Table 6.3: Energy calculations of  $H_2O$  in water ( $\epsilon_\infty = 78.304$ ), calculations with MRChem with  $\sigma \in \{0.5, 0.4, 0.3, 0.2\}$  and vacuum at absolute precisions  $10^{-2}$ ,  $10^{-3}$  and  $10^{-4}$

prec/ $\sigma$	$10^{-2}$	$10^{-3}$	$10^{-4}$
$g09_{vac}$	-76.057755	-76.065491	-76.067755
vac	-76.075838	-76.068214	-76.068199
$\Delta E_{0.5}$	0.019557	0.022781	0.023087
$\Delta E_{0.4}$	0.01509	0.020939	0.021132
$\Delta E_{0.3}$	0.000594	0.019195	0.019492
$\Delta E_{0.2}$	————	0.017729	0.017727
$\Delta E_{g09}$	0.014892	0.014806	0.014724
basis set	cc-pVTZ	cc-pVQZ	cc-pV5Z

All the calculations are performed with absolute accuracy  $10^{-2}$ ,  $10^{-3}$  and  $10^{-4}$ . The absolute precision parameter for MRChem means that the energy output energy have guaranteed. The precision parameter, however, does not say that the solvent energies are of that standard. To ensure better convergence, the precision for  $V$ -SCF was set to  $10 * prec$ . As an example; Looking at table 6.6 of  $CN^-$  calculations, we see that the energy calculations with  $\sigma = 0.4$  differ in the first digit when the accuracy is improved from  $10^{-2}$  to  $10^{-3}$ .

The calculations with higher accuracy ( $10^{-4}$ ) show a better trend, the effect of the solvent is consistently larger for  $\sigma = 0.5$  than for  $\sigma = 0.2$ . With this we can conclude that the effects of the solvent is larger when the slope is smoother.

Table 6.4: Energy calculations of  $NO^+$  in water ( $\epsilon_\infty = 78.304$ ), calculations with MRChem with  $\sigma \in \{0.5, 0.4, 0.3, 0.2\}$  and vacuum at absolute precisions  $10^{-2}$ ,  $10^{-3}$  and  $10^{-4}$

prec/ $\sigma$	$10^{-2}$	$10^{-3}$	$10^{-4}$
$g09_{vac}$	-128.969281	-128.979639	-128.981879
vac	-128.983688	-128.982300	-128.982208
$\Delta E_{0.5}$	0.1599829	0.180543	0.1806501
$\Delta E_{0.4}$	0.1667047	0.174443	0.1745618
$\Delta E_{0.3}$	0.1578163	0.169185	0.1693429
$\Delta E_{0.2}$	0.1665965	0.16469	0.1647211
$\Delta E_{g09}$	0.156288	0.155913	0.15578
basis set	cc-pVTZ	cc-pVQZ	cc-pV5Z

Table 6.5: Energy calculations of  $CH_3CONH_2$  in water ( $\epsilon_\infty = 78.304$ ), calculations with MRChem with  $\sigma \in \{0.5, 0.4, 0.3, 0.2\}$  and vacuum at absolute precisions  $10^{-2}$ ,  $10^{-3}$  and  $10^{-4}$

prec/ $\sigma$	$10^{-2}$	$10^{-3}$	$10^{-4}$
$g09_{vac}$	-208.061351	-208.077224	
vac	-208.102308	-208.081705	-208.081728
$\Delta E_{0.5}$	0.035670	0.037696	0.037730
$\Delta E_{0.4}$	0.028093	0.034525	0.034634
$\Delta E_{0.3}$	0.041725	0.031811	0.031682
$\Delta E_{0.2}$	0.061099	0.029635	—
$\Delta E_{g09}$	0.023664	0.023911	—
basis set	cc-pVTZ	cc-pVQZ	cc-pV5Z

When we compare the vacuum calculations and the ASC calculations with GAUSSIAN, the effect is further underlined. The difference between them is consistently lower than for the difference between vacuum and SVPE calculations. ( $\Delta E_{sol}^{vac}(MW) > \Delta E_{sol}^{vac}(GTO)$ )

The missing parts of the calculations are there for two reasons;

- The calculations with steep slope  $\sigma = 0.2$  with precision  $10^{-2}$  did not converge the potential. This is because of the numerical noise emerging when steep functions are represented with low accuracy in MWs.
- The calculations on relatively large molecules  $CH_3CONH_2$  in table ?? ran out of memory. The super computer Stallo was used, where the memory accessibilities of a student user was too small.

Table 6.6: Energy calculations of  $CN^-$  in water ( $\epsilon_\infty = 78.304$ ), calculations with MRChem with  $\sigma \in \{0.5, 0.4, 0.3, 0.2\}$  and vacuum at absolute precisions  $10^{-2}$ ,  $10^{-3}$  and  $10^{-4}$

prec/ $\sigma$	$10^{-2}$	$10^{-3}$	$10^{-4}$
$g09_{vac}$	-92.333965	-92.344713	-92.348284
vac	-92.348222	-92.349717	-92.349648
$\Delta E_{0.5}$	0.134355	0.123122	0.123183
$\Delta E_{0.4}$	0.016045	0.122701	0.122856
$\Delta E_{0.3}$	0.134171	0.122398	0.122574
$\Delta E_{0.2}$	—	0.121673	0.122198
$\Delta E_{g09}$	0.12337	0.121018	0.11925
basis set	cc-pVTZ	cc-pVQZ	cc-pV5Z

## 6.2.2 Solvent dipole Moment

Table 6.7: Dipole moment calculations of  $H_2O$  in water ( $\epsilon_\infty = 78.304$ ), calculations with MRChem with  $\sigma \in \{0.5, 0.4, 0.3, 0.2\}$  and vacuum at absolute precisions  $10^{-2}$ ,  $10^{-3}$  and  $10^{-4}$

prec/ $\sigma$	$10^{-2}$	$10^{-3}$	$10^{-4}$
$g09_{vac}$	0.782591	0.775323	0.772920
vac	0.766106	0.764234	0.764085
$\Delta\mu_{0.5}$	-0.258606	-0.26051	-0.260437
$\Delta\mu_{0.4}$	-0.244328	-0.250666	-0.239371
$\Delta\mu_{0.3}$	-0.213728	-0.239243	-0.250424
$\Delta\mu_{0.2}$	—	-0.227844	-0.227657
$\Delta\mu_{g09}$	-0.175628	-0.188796	-0.194355
basis set	cc-pVTZ	cc-pVQZ	cc-pV5Z

The dipole moment where calculated as:

$$\vec{\mu} = \int \vec{r} \rho_{tot}(r) dr \quad (6.1)$$

where  $\vec{r}$  is the position operator and  $\vec{\mu}$  a vector. The norm of the vectors are reported in table 6.7 and show the same trend as for the energy calculations. Steeper slope gives less impact of the solvent.

Table 6.8: Spillover effect, calculated with HF  $H_2O$ , with precision  $10^{-2}$ ,  $10^{-3}$  and  $10^{-4}$  and slope  $\sigma = 0.2, 0.3, 0.4$ 

prec/ $\sigma$	$10^{-2}$	$10^{-3}$	$10^{-4}$
0.2		.153 196	.153 135
0.3	.134 079	.137 216	.137 190
0.4	.123 330	.123 810	.123 779
0.5	.112 253	.112 527	.112 522

### Spillover

The spillover effect shows that more of charge density is located outside the van der Waals (vdW) radius when the slope is steeper. This is an effect of having a dielectric function ( $\varepsilon(r)$ ) that is not symmetric around the radius of the sphere. The effect is consistent with the energy and dipole moment calculations.

## 6.3 Concluding remarks and ideas for improvement

The implementations of  $V$ -SCF gives good insight in the possibilities that resides within the MW framework implemented in MRCHEM . The implementations was shown to give consistent results with that of highly tested programs like GAUSSIAN.

The pilot implementation of the code gives hope of further improvement. One idea is too give  $\gamma$  a new representation by;

$$\nabla\varepsilon(r)/\varepsilon(r) = \nabla\log\left(\frac{\varepsilon_0}{\varepsilon_\infty}\right)\nabla C(r) = \nabla\log(\varepsilon(r)) \quad (6.2)$$

The idea is; since the function values of  $C(r)$  resides in  $(0, 1)$ , it is a smoother function than  $\varepsilon(r)$ . Which is easier to represent and thereby easier to differentiate than  $\varepsilon(r)$ . In theory, this should give better convergence.

Another idea is to use variational representation of the algorithm  $V$ -SCF.

# Bibliography

- [1] Multiresolution chemistry (mrchem) program package. <http://mrchemdoc.readthedocs.org/en/latest/>, 2017.
- [2] MJE Frisch, GW Trucks, Hs B Schlegel, GE Scuseria, MA Robb, JR Cheeseman, G Scalmani, V Barone, B Mennucci, GA Petersson, et al. Gaussian 09, revision d. 01, 2009.
- [3] Erich Zauderer. *Partial differential equations of applied mathematics*, volume 71. John Wiley & Sons, 2011.
- [4] Robert R Schaller. Moore's law: past, present and future. *IEEE spectrum*, 34(6):52–59, 1997.
- [5] Peter W Atkins and Ronald S Friedman. *Molecular quantum mechanics*. Oxford university press, 2011.
- [6] Stig Rune Jensen, Santanu Saha, José A Flores-Livas, William Huhn, Volker Blum, Stefan Goedecker, and Luca Frediani. The elephant in the room of density functional theory calculations. *The Journal of Physical Chemistry Letters*, 8(7):1449–1457, 2017.
- [7] Alfred Haar. Zur theorie der orthogonalen funktionensysteme. *Mathematische Annalen*, 69(3):331–371, 1910.
- [8] Wolfram Research, Inc. Mathematica, Version 11.2. Champaign, IL, 2017.
- [9] Kestutis Aidas, Celestino Angeli, Keld L Bak, Vebjørn Bakken, Radovan Bast, Linus Boman, Ove Christiansen, Renzo Cimiraglia, Sonia Coriani, Pål Dahle, et al. The dalton quantum chemistry program system. *Wiley Interdisciplinary Reviews: Computational Molecular Science*, 4(3):269–284, 2014.

- 
- [10] Stig Rune Jensen, Jonas Jusélius, Antoine Durdek, Tor Flå, Peter Wind, and Luca Frediani. Linear scaling coulomb interaction in the multi-wavelet basis, a parallel implementation. *International Journal of Modeling, Simulation, and Scientific Computing*, 5(supp01):1441003, 2014.
- [11] Robert J Harrison, Gregory Beylkin, Florian A Bischoff, Justus A Calvin, George I Fann, Jacob Fosso-Tande, Diego Galindo, Jeff R Hammond, Rebecca Hartman-Baker, Judith C Hill, et al. Madness: A multi-resolution, adaptive numerical environment for scientific simulation. *SIAM Journal on Scientific Computing*, 38(5):S123–S142, 2016.
- [12] R Ditchfield. Molecular orbital theory of magnetic shielding and magnetic susceptibility. *The Journal of Chemical Physics*, 56(11):5688–5691, 1972.
- [13] Stig Rune Jensen, Tor Flå, Dan Jonsson, Rune Sørland Monstad, Kenneth Ruud, and Luca Frediani. Magnetic properties with multiwavelets and dft: the complete basis set limit achieved. *Physical Chemistry Chemical Physics*, 18(31):21145–21161, 2016.
- [14] Trygve Helgaker, Poul Jorgensen, and Jeppe Olsen. *Molecular electronic-structure theory*. John Wiley & Sons, 2014.
- [15] Attila Szabo and Neil S Ostlund. *Modern quantum chemistry: introduction to advanced electronic structure theory*. Courier Corporation, 2012.
- [16] Frank Jensen. *Introduction to computational chemistry*. John wiley & sons, 2017.
- [17] Stig Rune Jensen. Real-space all-electron density functional theory with multiwavelets. 2014.
- [18] Carl Norling and Jonny Österman. Physics handbook for science and engineering. *Studentlitteratur, Lund, Sweden*, 2002.
- [19] Wolfgang Pauli. Über den zusammenhang des abschlusses der elektro-nengruppen im atom mit der komplexstruktur der spektren. *Zeitschrift für Physik A Hadrons and Nuclei*, 31(1):765–783, 1925.
- [20] Clemens Carel Johannes Roothaan. New developments in molecular orbital theory. *Reviews of modern physics*, 23(2):69, 1951.
- [21] GG HALL. The molecular orbital theory of chemical valency viii. a method of calculating ionization potentials.

- 
- [22] Simen Reine and Trond Saue. European summerschool in quantum chemistry.
- [23] Pierre Hohenberg and Walter Kohn. Inhomogeneous electron gas. *Physical review*, 136(3B):B864, 1964.
- [24] Walter Kohn and Lu Jeu Sham. Self-consistent equations including exchange and correlation effects. *Physical review*, 140(4A):A1133, 1965.
- [25] Richard A Bryce, Robert Buesnel, Ian H Hillier, and Neil A Burton. A solvation model using a hybrid quantum mechanical/molecular mechanical potential with fluctuating solvent charges. *Chemical physics letters*, 279(5-6):367–371, 1997.
- [26] Eliot Boulanger and Walter Thiel. Solvent boundary potentials for hybrid qm/mm computations using classical drude oscillators: a fully polarizable model. *Journal of chemical theory and computation*, 8(11):4527–4538, 2012.
- [27] Dirk Bakowies and Walter Thiel. Hybrid models for combined quantum mechanical and molecular mechanical approaches. *The Journal of Physical Chemistry*, 100(25):10580–10594, 1996.
- [28] Maarten TP Beerepoot, Arnfinn Hykkerud Steindal, Nanna Holmgaard List, Jacob Kongsted, and Jogvan Magnus Haugaard Olsen. Averaged solvent embedding potential parameters for multiscale modeling of molecular properties. *Journal of chemical theory and computation*, 12(4):1684–1695, 2016.
- [29] Geoffrey Dutton. Encoding and handling geospatial data with hierarchical triangular meshes. In *Proceeding of 7th International symposium on spatial data handling*, volume 43. Netherlands: Talor & Francis, 1996.
- [30] <http://montage.ipac.caltech.edu/docs/WWT/>, 4/11-2017.
- [31] Jacob Fosso-Tande and Robert J Harrison. Implicit solvation models in a multiresolution multiwavelet basis. *Chemical Physics Letters*, 561:179–184, 2013.
- [32] Thomas Williams, Colin Kelley, and many others. Gnuplot 5.0: an interactive plotting program. <http://gnuplot.sourceforge.net/>, November 2017.
- [33] R Di Remigio, TD Crawford, and L Frediani. Pcmsolver: An application programming interface for the polarizable continuum model, 2016.

- [34] Robert J Harrison. Krylov subspace accelerated inexact newton method for linear and nonlinear equations. *Journal of computational chemistry*, 25(3):328–334, 2004.
- [35] RBS Krishnan, J Stephen Binkley, Rolf Seeger, and John A Pople. Self-consistent molecular orbital methods. xx. a basis set for correlated wave functions. *The Journal of Chemical Physics*, 72(1):650–654, 1980.